

RNI: DELENG/2005/15153
Publication: 23rd of every month
Posting: 27th/28th of every month at DPSO

No: DL(E)-01/5079/2023-25
Licensed to post without pre-payment U(E) 28/2023-25
Rs.150

ISSN 0973-2136

www.mycoordinates.org

Coordinates

Volume XX, Issue 5, May 2024

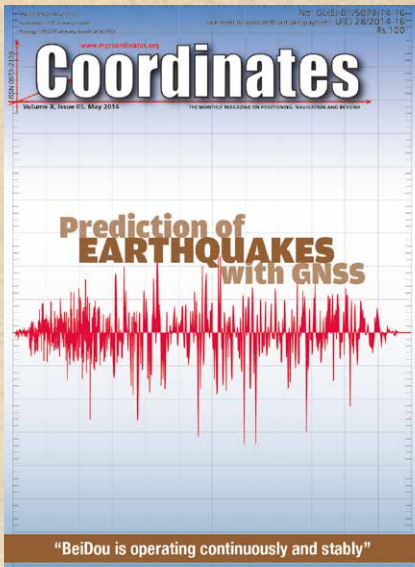
THE MONTHLY MAGAZINE ON POSITIONING, NAVIGATION AND BEYOND

WILdetect

An intelligent platform to perform
airborne wildlife census automatically
in the marine ecosystem

Towards automated nautical chart compilation and
verification of output topology and safety

In Coordinates



mycoordinates.org/vol-X-issue-5-May-2014

Suitability of projection for Defense Series Maps

Lt Col PVGS Jayaram, General Staff Officer (Software & GIS), Project Management Organisation, Directorate General of Information Systems, Integrated Headquarters of Ministry of Defence, New Delhi, India

Dr T Vijaya Lakshmi, Assistant Professor, Dept of Environment, Institute of Science and Technology, JNTUH, Hyderabad, India

Maj Gen RC Padhi, Additional Surveyor General & Head, Indian Institute of Surveying and Mapping, Hyderabad, India

It's right time to close the discussion once for all and cement the choice of suitable projection for DSM. National Mapping Policy 2005 has recommended rightfully the usage of UTM as projection for Open Series Maps (OSM), and LCC for Defence Series Maps (DSM).

10 years before... Towards the prediction of Earthquakes with GNSS data

Dr Shunji Murai, Professor Emeritus, University of Tokyo, Japan and Advisor to Japan Earthquake Science Exploration Agency (JESEA)

Dr Harumi Araki, Head, Environmental Geological Laboratory, Japan and Advisor to JESEA

Dr Hideharu Yanagi, Chief Researcher, JESEA, Japan

The objective of the study is to detect signals before the Great Earthquake using various indicators computed from the daily GNSS data, with a view to their being used in future for the prediction of earthquakes. The study succeeded to detect several pre-signals six months, five months, one month and three days before the Great Earthquake in the daily data, averaged weekly data, weekly maximum deviations, height changes over two years and/or accumulated changes.

Precision analysis of IGS long baseline Processing based on GAMIT/GLOBK

Erhu WEI, PhD, Professor, PhD supervisor, School of Geodesy and Geomatics, Laboratory of Geospace Environment and Geodesy, Ministry of Education, Wuhan University, Wuhan, China

Jiandong LIU, Master Candidate, School of Geodesy and Geomatics, Wuhan University, Wuhan, China

The paper expounds the main module of GAMIT GPS data processing software, basic steps and treatment scheme of the data processing and quality evaluation system of the GAMIT data processing. This paper introduces the main application, steps of data processing of the software GLOBK and the problems that people need to be aware of.

Tutankhamun's father - Akhenaten's city of the sun

John Francis Brock, Director, Brock Surveying, Australia

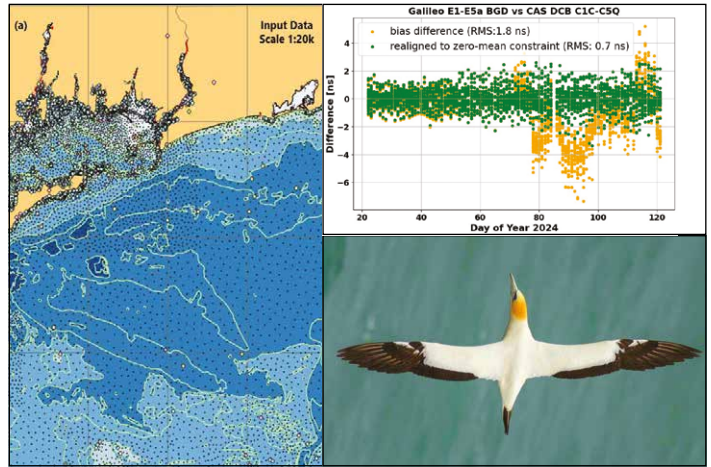
The paper describes the design and layout of these impressive ancient surveyor's boundary stones along with contemporary history leading up to the most recent events affecting Akhenaten's Stelae as a spectacular example of the vital importance of surveyors during this turbulent period of the Great Egyptian Civilisation.

Search for the plate transition zone in Bulgaria with GPS

Keranka Vassileva and Mila Atanasova-Zlatareva

National Institute of Geophysics, Geodesy and Geography, Bulgarian Academy of Sciences, Sofia, Bulgaria

The main objectives of this study are the estimation of Euler rotation vector and Euler pole and on the base of obtained results to attempt to determine the transition boundary of the Eurasia plate in the Bulgarian territory.



In this issue

Coordinates Volume 20, Issue 5, May 2024

Articles

Towards automated nautical chart compilation and verification of output topology and safety TAMER NADA, CHRISTOS KASTRISIOS, BRIAN CALDER, CHRISTIE ENCE, CRAIG GREENE AND AMBER BETHELL 5
GNSS Constellation Specific Monthly Analysis Summary: April 2024 NARAYAN DHITAL 14
WILDetect: An intelligent platform to perform airborne wildlife census automatically in the marine ecosystem KAYA KURU, STUART CLOUGH, DARREN ANSELL, JOHN MCCARTHY AND STEPHANIE MCGOVERN 19

Columns

Old Coordinates 2 **My Coordinates** EDITORIAL 4 **News** GNSS 18 IMAGING 30 GIS 31 UAV 32 INDUSTRY 32
MARK YOUR CALENDAR 34

This issue has been made possible by the support and good wishes of the following individuals and companies

Amber Bethell, Brian Calder, Christie Ence, Christos Kastrisios, Craig Greene, Darren Ansell, John McCarthy, Kaya Kuru, Narayan Dhital, Stephanie McGovern, Stuart Clough and Tamer Nada; SBG System, and many others.

Mailing Address

A 002, Mansara Apartments
C 9, Vasundhara Enclave
Delhi 110 096, India.

Phones +91 11 42153861, 98102 33422, 98107 24567

Email

[information] talktous@mycoordinates.org

[editorial] bal@mycoordinates.org

[advertising] sam@mycoordinates.org

[subscriptions] iwant@mycoordinates.org

Web www.mycoordinates.org

Coordinates is an initiative of CMPL that aims to broaden the scope of positioning, navigation and related technologies.

CMPL does not necessarily subscribe to the views expressed by the authors in this magazine and may not be held liable for any losses caused directly or indirectly due to the information provided herein. © CMPL, 2024. Reprinting with permission is encouraged; contact the editor for details.

Annual subscription (12 issues)

[India] Rs.1,800* [Overseas] US\$100*

*Excluding postage and handling charges

Printed and published by Sanjay Malaviya on behalf of Coordinates Media Pvt Ltd

Published at A 002 Mansara Apartments, Vasundhara Enclave, Delhi 110096, India.

Printed at Thomson Press (India) Ltd, Mathura Road, Faridabad, India

Editor Bal Krishna

Owner Coordinates Media Pvt Ltd (CMPL)

This issue of Coordinates is of 36 pages, including cover.

GPT-4o: Engaging with Conversational AI

OpenAI unveils GPT-4o,
The latest iteration of AI chatbot technology,
Promising enhanced speed, advanced capabilities,
And an engaging conversational style.
Real time interaction, image recognition, language translation,
And interestingly, emotion detection
A significant advancement in man-machine interaction,
When machine will understand human emotions.
With apparent promises of positive social impacts,
Greater are the worries regarding data privacy,
Potential of misinformation, manipulation and biases,
With plethora of ethical issues such as consent and exploitation,
Especially with vulnerable groups like children,
And people with cognitive impairment.

Bal Krishna, Editor
bal@mycoordinates.org

ADVISORS Naser El-Sheimy PEng, CRC Professor, Department of Geomatics Engineering, The University of Calgary Canada, George Cho Professor in GIS and the Law, University of Canberra, Australia, Professor Abbas Rajabifard Director, Centre for SDI and Land Administration, University of Melbourne, Australia, Luiz Paulo Souto Fortes PhD Associate Professor, University of State of Rio Janeiro (UERJ), Brazil, John Hannah Professor, School of Surveying, University of Otago, New Zealand

Towards automated nautical chart compilation and verification of output topology and safety

In this paper, we discuss a research effort for an Automated Nautical-chart Generalization (ANG) model in the Esri environment

Tamer Nada

Center for Coastal and Ocean Mapping/
UNH-NOAA Joint Hydrographic Center,
University of New Hampshire, Durham, USA

Christos Kastrisios

Center for Coastal and Ocean Mapping/
UNH-NOAA Joint Hydrographic Center,
University of New Hampshire, Durham, USA

Brian Calder

Center for Coastal and Ocean Mapping/
UNH-NOAA Joint Hydrographic Center,
University of New Hampshire, Durham, USA

Christie Ence

NOAA, Office of Coast Survey, Marine
Chart Division, Silver Spring, MD, USA

Craig Greene

Esri, Marine & Topographic Production
Division, Redlands, CA, USA

Amber Bethell

Esri, Marine & Topographic Production
Division, Redlands, CA, USA

Abstract

The compilation of Electronic Navigational Charts (ENCs) requires significant amount of time, labor-intensive efforts, and cost. Despite the advancements in technology and the various research efforts, generalization tasks are still performed manually or semi-manually with expected human errors. The dramatic increase in the amount of data that is collected by modern acquisition systems, in addition to the increasing timeline expected by the end-users, are constantly driving Hydrographic Offices (HOs) toward the investigation and adoption of more advanced and effective ways for automating the generalization tasks to speed up the process, minimize the cost, and improve productivity. Full automation of the nautical chart compilation process has been unreachable due to the strict nautical cartographic constraints (and particularly those of safety and topology) that pose a challenge for most of the available generalization tools, while it remains questionable whether automation can replace human thought processes. In this paper, we discuss a research effort for an Automated Nautical-chart Generalization (ANG) model in the Esri environment. The ANG model builds upon the nautical chart generalization guidelines and practice and utilizes available tools in the Esri environment to perform the generalization of selected ENC features to the target scale. Safety constraints in the marine domain is of utmost importance, however, since most of the readily available tools

do not respect safety, the main goal of this effort has been an output with no topological violations. In the current phase of the project, we evaluate safety of soundings and contour for user fixing and while the validation of bathymetry is a well-researched topic, there was the need for an automated process to identify the sections of the generalized contours that have been displaced toward the shallow water side. Therefore, this work also presents a safety validation tool that detects the contours' safety violations in the output. The tool is composed of three main stages that run individually after the ANG model is complete with the aim to highlight the safety violations for fixing by cartographers.

1. Introduction

The Electronic Navigational Chart (ENC) is a Digital Landscape Model which is converted to a Digital Cartographic Model when rendered on the Electronic Chart Display Systems (ECDISs) (Dyer et al., 2022). It is a database that comprises numerous point feature objects (e.g., soundings, navigational aids), line objects (e.g., depth contours, coastlines) and polygons (e.g., depth areas, land areas) which are encoded using the chain-node topology and are important for the safety of ship navigation (IHO, 2020). ECDIS integrates ENCs, navigating related system and sensors aboard ships to give mariners complete picture of the instantaneous situation of the vessel and charted dangers in the area

(Alexander, 2003). In many Hydrographic Offices (HOs) ENC features were compiled for years directly from the existing paper charts with digitization. Consequently, nowadays, most of the available ENCs are based on the footprints of the paper charts from which they were derived (Kastrisios and Calder, 2018). This is the main reason for the existing horizontal and vertical inconsistencies between adjacent cells, which may confuse mariners and reduce their confidence in the nautical chart. In addition, inconsistencies can affect the performance of ECDIS that uses the data for analysing the safety of the vessels underway, either by triggering false alarms that might contribute to the situation called “mariner’s deafness”. i.e., the situation where the mariner disregard important alarms because of a considerable number of irrelevant ones (Kastrisios, Calder and Bartlett, 2020), or, even worse, may lead to a system crash. Furthermore, as per the IHO standards for nautical charting (IHO, 2020), six usage bands exist, each associated with the intended navigational use (i.e., overview, general, coastal, approach, harbour, and berthing) and the radar range. Therefore, HOs are required to produce, maintain, update, and deliver a large portfolio of ENC bands in support of safety of navigation in a timely and consistent manner, which is considered a tedious and time-consuming process.

On the other hand, the International Hydrographic Organization (IHO) is encouraging HOs to update their current coverage schema (IHO, 2021) from the puzzle-piece layout resulted from the paper-chart-first concept, (e.g., Figure 1a) to a rectangular gridded system (e.g., Figure 1b). In 2019, the Office of Coast Survey (OCS) of the USA National Oceanic and Atmospheric Administration (NOAA), started

rescheming their ENC suite by creating a gridded system with standardized scales and cell sizes. The standard scales follow a dyadic system in which each successively smaller scale is half of the preceding scale, and cell boundaries follow lines of longitude and latitude to appear as rectangular on a Mercator projection (e.g., Figure 1b). (NOAA, 2019)

The new gridded NOAA ENC coverage approach aims to significantly reduce the number of current chart scales, produce larger and standard scale coverage, facilitate metrification for NOAAs’ charts and resolve vertical and horizontal inconsistency (NOAA, 2019). The project, which is expected to take years to complete, would benefit greatly from automation of individual generalization tasks, or, should this be possible, the entire process.

A fully automated solution for generating nautical charts from the highest level of detail data, to the appropriate scale, can streamline and minimize the time and effort needed for chart production. Respecting the nautical charts constraints, i.e., legibility, morphology, topology, and safety and especially the latter, is the main reason why current generalization processes and algorithms developed for land mapping are not directly applicable to the maritime domain and safety of navigation related products.

In this paper, we present an Automated Nautical-chart Generalization (ANG) model in the Esri environment that builds upon a set of constrains, extracted from the available nautical cartographic specifications, categorized and translated into rules to be defined in a template as conditions to be respected during the generalization process. The model aims to describe and implement the generalization steps from the highest level of detail ENC data to the target scale with no topological errors. However, since safety is of utmost importance and there are no readily available algorithms that fully respect its relevant constraints, a validation tool is developed and presented that detects all safety violation in the ANG model output and highlight it for user fixing. This tool can be used to validate safety even when new fully safe generalization algorithms are available.

A fully automated solution for generating nautical charts from the highest level of detail data, to the appropriate scale, can streamline and minimize the time and effort needed for chart production

2. Background

Generalization process and algorithms developed for topographic maps are different than those for nautical charts. In other words, it is mostly not applicable to the marine domain due to safety of navigation. For instance, in nautical charts generalization, depth contours are only allowed to move to the deep side during generalization (see Figure 3), this is to guarantee that a ship never runs aground because of miss representation (Peters et al., 2014). There are four types of constraints that need to be respected for the generalization of a nautical chart:

- *Topology* (e.g., no gaps or overlaps between skin of the earth features).
- *Safety* (e.g., Shallow depths need to be maintained and at every location, the indicated depth must not be deeper than the depth

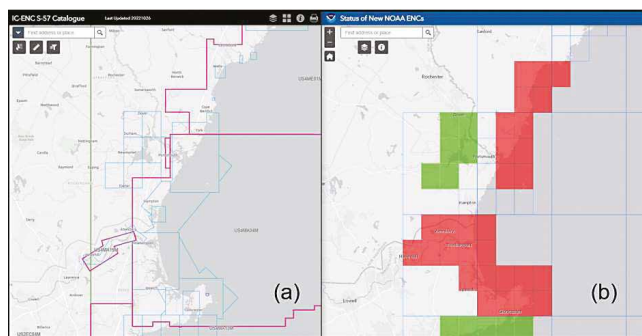


Figure 1. Current and planned gridded scheme for different usage bands, US East-Coast Newburyport (a) IC-ENC S-57 Catalogue (IC-ENC, 2022) (b) Status of New NOAA ENCs (NOAA, 2022)

that was originally measured at that location). (Figure 2)

- **Legibility** (e.g., only essential information should be shown in a clear and efficient way).
- **Morphology** (e.g., slope and roughness of the seafloor must be maintained as much as possible). (Peters et al., 2014)

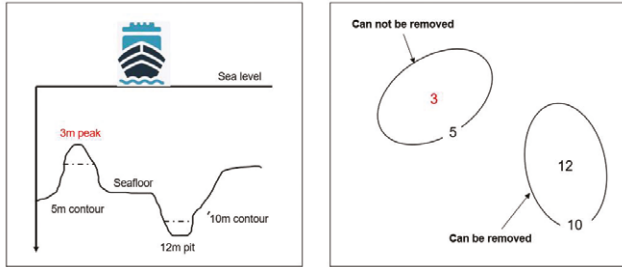


Figure 2. Illustration of Safety constraint, modified from Zhang and Guilbert (2011)

Those four constraints are sometimes incompatible with each other. Some are absolute, while others have a degree of flexibility. The first two are considered more strict (i.e., hard constraints) and should be mostly satisfied and hardly violated for the chart to be valid. In other words, constraints do not have the same degree of importance, thus, during the generalization process, compromises must be made. For example, the morphology constraint indicates to maintain the morphology of the sea floor and stay close to its measured shape as much as possible, whereas the legibility constraint deviates from this by disregarding details (Zhang & Guilbert, 2011).

3. Related work

Various research efforts have tried to automate individual nautical chart generalization tasks. For instance, in sounding selection the works by Zoraster and Bayer (1992), Tsoulos and Stefanakis (1997), Sui et al. (2005), Owens and Brennan (2012), Yu (2018), Lovrinčević (2019), Skopeliti et al. (2020), and Dyer, et al. (2022). In Depth contours generalization, those by Guilbert and Lin (2006), Guilbert and Zhang (2012), Miao and Calder (2013), Peters et al. (2014), Yan et al. (2017), Skopeliti et al. (2021). Other works have focused on validating the safety (e.g., Wilson et al. (2017), Kastrisios and Calder

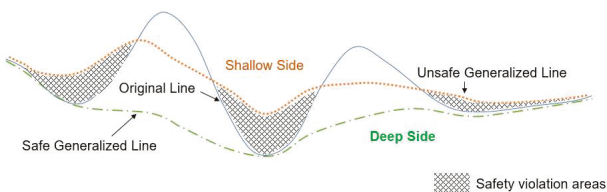


Figure 3. Illustration of the depth curve generalization safety constraint, modified from Guilbert and Lin (2006)

(2018), Kastrisios et al. (2019a) and Dias et al. (2022)), and topology of depth information on charts, (e.g., Kastrisios et al. (2020) and Huo et al. (2022)). In addition, a number of available software applications perform S-58 validation checks and provide reports on Group 1 and Group 2 objects (e.g., Esri ArcGIS Maritime, Teledyne CARIS S-57 composer, SevenCs Analyzer and C-Map dKart Inspector) (Kastrisios and Calder, 2020). In 2013, Socha and Stoter introduced a research effort for automating nautical chart production. The research main goal was defining computer translatable rules

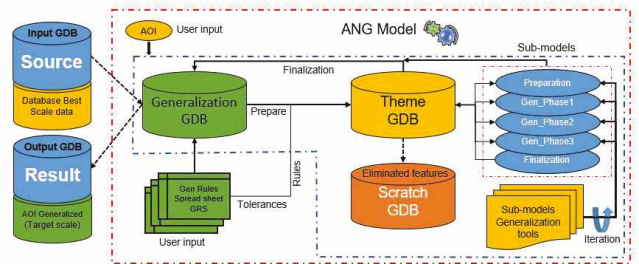


Figure 4. schematic description of the Automated Nautical Generalization Model (Nada et al., 2022)

for creating small scale ENC's (i.e., coastal) from higher scale (i.e., approach) with minimal human intervention. The study focused on nine ENC feature classes (Socha and Stoter, 2013).

4. The Automated Nautical-chart Generalization model (ANG)

The Automated Nautical Generalization model is developed in the Esri environment. As shown in Figure 4, it utilizes the generalization rules spreadsheet, which is generated from the input database schema and the nautical constraint template (see section 4.1 & 4.2), as the input that drives the data generalization for any desired output scale, using the ArcGIS Pro available generalization algorithms and tools. (Nada et al., 2022)

There are more than 170 geo-features defined for ENC's as per the IHO standards S-57/101 (IHO, 2018). These features

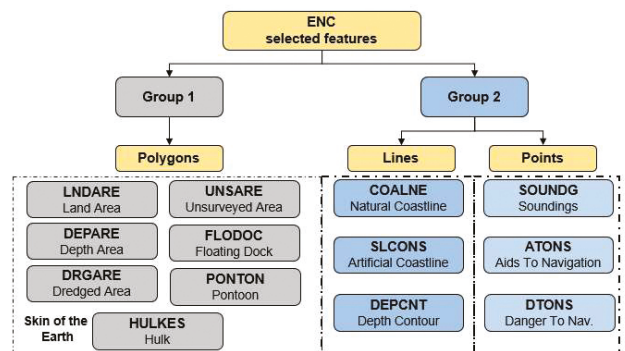


Figure 5. ENC selected S-57/101 features and associated NIS Feature class

are categorized under the three geometric primitives (i.e., points, lines and polygons). In this research work, a number of features were selected for the proof of concept. As shown in Figure 5, the selected features are the seven polygonal feature classes representing the Skin of the Earth (Group1), and six related group of features that belong to S-57 features classes (i.e., natural coastline “COALNE”, artificial coastline “SLCONS”, depth contour “DEPCNT”, sounding “SOUNDG”) and NOAA Nautical Information System (NIS) feature class group (i.e., aids to navigation “ATONS”, danger to navigation “DTONS”). The NIS is a multi-scale attributed geospatial database, primarily used for NOAA ENC maintenance and publication utilizing Esri ArcGIS (Ence, 2018).

4.1 The Generalization Constraint Template

From the available nautical cartographic standards, e.g., S-4 Regulations of the IHO for International Charts and Chart Specifications (IHO, 2020), and NOAA Nautical Chart Manual, Policies and Procedures (NOAA, 2019), a template was developed to categorize and define the properties of the nautical constraints as conditions to be respected during the generalization process. The template includes the geometry type, feature class and value for each condition. This value does not represent sequence but rather the hierarchy, i.e., the degree of importance, of those conditions (Nada et al., 2023b).

4.2 The Generalization Rules Spreadsheet

The generalization rules spreadsheet (GRS) is an excel spreadsheet that is used to configure the ANG model. It is developed from the nautical constraints template to match the input database schema. The GRS is composed of several tabs that contain all the required information about the selected feature classes, e.g., the geometric and generalization relationship between features, the tolerances to be used for the target scale, hierarchy levels and operations that needs to be implemented on each feature (Nada et al., 2023).

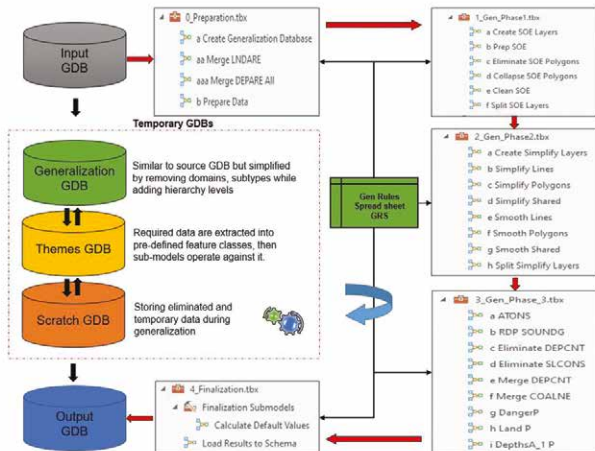


Figure 6. The Generalization Phases in ArcGIS Pro

4.3 The ANG model Generalization Phases

The ANG model is organized in five main phases or sub-models (Figure 6); each phase consists of various generalization tools that are used to automate the process. The GRS drives the data generalization for the desired output scale.

4.3.1 Preparation phase

A series of steps are taken before running the ANG model to prepare the input geo-database GDB as follows:

1. An empty GDB is created in ArcGIS Pro.
2. The GDB schema is developed using a pre-configured ENC schema in a workspace xml format that contains all the required feature classes, tables, spatial attributes used to capture ENC information in a GDB schema (Esri, 2022).
3. The Generalization Rules template is then created based on the configured GDB schema to build the GRS rule file.
4. The area of interest (AOI) highest level of detail available ENCs are loaded to the configured GDB.
5. The research selected feature classes (Figure 5) are imported from the loaded ENCs to the configured input GDB.
6. The GRS is validated using the Generalization Rule Validation tools in ArcGIS Pro (Esri, 2021) to confirm that all tolerances and rules have been defined for the target scale.

Once the previous steps are taken by the user, the ANG model runs creating a number of GDBs that will be used throughout the generalization process, each has a specific role as follows:

- A Generalization GDB that has a similar schema to the input GDB but simplified and optimized for generalization within the AOI by removing domains, subtypes, and topologies not being used by the model. This GDB is used to backup the data after each generalization phase.

Table 1. The Geometric & Generalization relationship defined in the GRS

Class Relation	Description	Valid Geometry
Geometric		
SOE	Skin of the Earth features	Polygon
Interior	Features contained within a SOE polygon.	Line
Edge	Features that share a coincident edge within an SOE polygon (e.g., Coastline features)	Line
Generalization		
Individual	Features generalized individually..	Line - Polygon
Shared	Features that contain shared edges that should be generalized together.	Line - Polygon
Barrier	Features used as barriers to maintain topological relationships when Individual and Shared features are processed.	Point - Line - Polygon

- A Theme GDB which is used to extract the required and pre-defined feature classes from the generalization GDB and apply the assigned generalization operations on it.
- A Scratch GDB which is used for storing temporary and eliminated data during the generalization process.
- The Result GDB will be created by the Finalization sub-model to match the input GDB schema. After all the sub-models have run, the generalized data are extracted from the generalization GDB and copied to this GDB adding all the attributes that have been simplified in the generalization GDB.

4.3.2 Generalization first phase P1G

In the first generalization phase, Group 1 polygons (see Figure 5) that fall under the area tolerance defined in the GRS are either collapsed to points or eliminated. Those features are extracted from the generalization GDB, converted to the theme-based schema and exported to the Theme GDB. As illustrated in Table 1, the generalization and geometric relationship between features are extracted from the GRS and assigned to the selected features. This pre-defined relationship between selected features is a key to the whole process. Each feature is assigned a geometric (e.g., SOE) and a generalization relation (e.g., Shared) that control how features interact during the generalization phases. The final stage in P1G is to clean and split features by dissolving and filling gaps, as well as removing any SOE edge lines where polygons were dissolved. The output of P1G is polygons without topological violations which are stored in the Theme GDB and backed up in the Generalization GDB.

4.3.3 Generalization Second phase P2G

The second generalization phase is responsible for simplifying and smoothing the selected features. Based on the rules defined in the GRS, shared features are loaded to the Theme GDB and generalized by the assigned tool. For instance, the *Simplify Shared* tool extracts the shared simplification tolerances from the GRS, iterate through the selected features and runs *Simplify Shared Edges* on the specified features, using other features as barriers (Nada et al., 2023b).

4.3.4 Generalization third phase P3G

The third generalization phase is responsible for generalizing interior, individual and barrier lines and points (see Table 1). For example, dissolving and merging of DEPCNTs, selection of SOUNDGs and ATONS. Barrier features' positions are respected during the generalization process by higher agents (i.e., Polygons - Lines). For instance, a DEPCNT will not cross any SOUNDGs or ATONS on both sides of the contour when being processed, this might restrict the amount of simplification, or be judged as under generalization, but will prevent having a deep SOUNDG on a shallow side and vice versa.

4.3.5 Finalization phase

In the finalization phase, an output GDB is created and

the generalized features will be loaded to it from the Generalization GDB matching the input GDB schema. This would include adding the domains, subtypes and default values that were simplified in the Preparation Phase.

5. Implementation

The ANG model was tested in a number of locations, with different real world scenarios (e.g., with and without edge matching inconsistency - mix of scale bands), to generalize band 5 (i.e., 20k) to band 4 (i.e., 80k) data. The model output GDBs in all scenarios showed no topological violations (see Nada et al., 2023b).

Figure 7 illustrates the model results in the case with no edge matching inconsistency (i.e., New York – Block Island

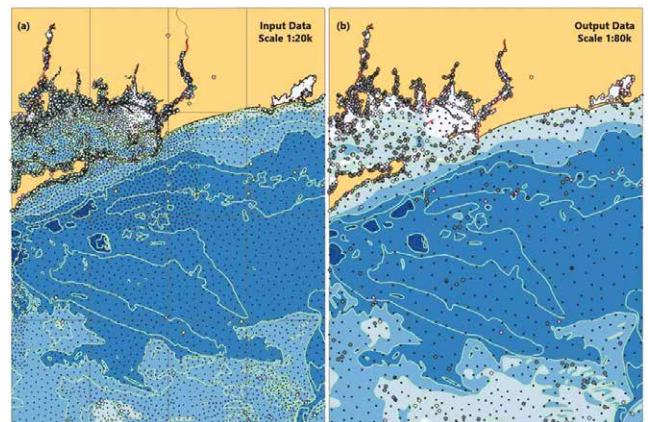


Figure 7. The study area – Block Island, NY-USA (a) Before generalization (b) After generalization

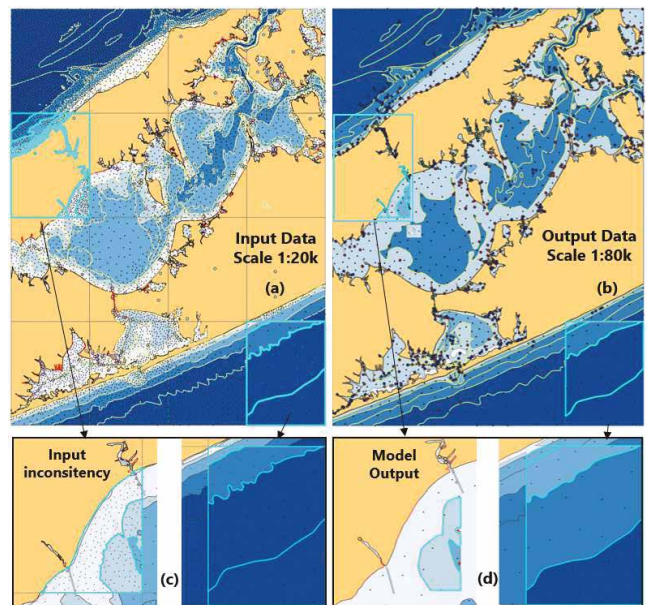


Figure 8. The study area – Long Island Sound, NY-USA (a) Pre-generalization data (b) Post-generalization data (c) Input inconsistency cells (d) Inconsistency model output

Sound area). The model was able to generalize the selected features from 16 band 5 ENC's (Figure 7a) at scale 1:20k to scale 1:80k (Figure 7b) with no topological errors.

Figure 8 illustrates the model results in the case with a couple of edge matching inconsistent cells (i.e., New York, Long Island Sound area). In this case, selected features (see figure 5) from 16 band 5 ENC's (Figure 8a) were used as the input GDB. The model was able to generalize the selected features, as per the tolerances defined in the GRS, with no topological violations (Figure 8b). However, there were a few instances of edge matching inconsistencies in two of the 16 cells (highlighted in Figure 8a & 8b) that

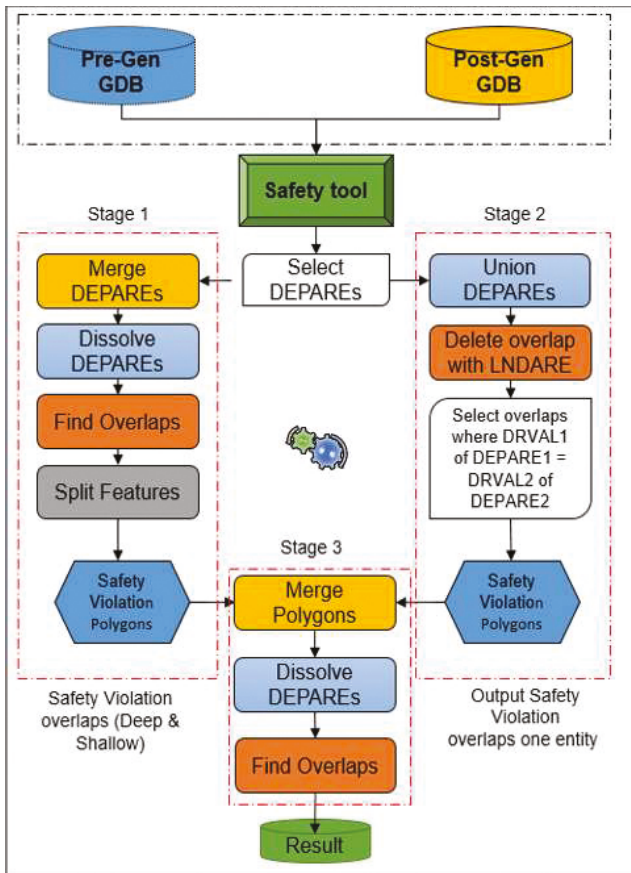


Figure 9. Safety Validation tool flowchart with the three main stages

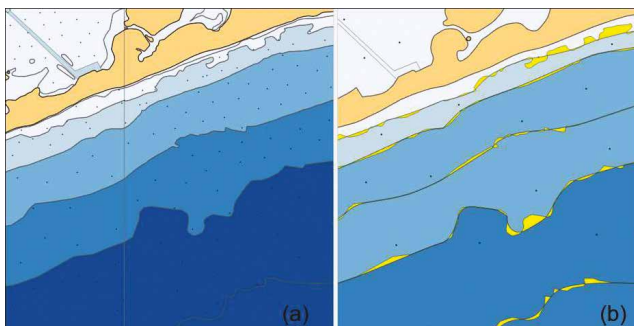


Figure 10. Safety Validation first stage results – Pre and Post generalization differences

did not share end point topology and where the model was unable to merge or dissolve the respective line and polygonal features. These features were treated and generalized separately from the ANG Model (Figure 8c & 8d).

6. Validation tools

As explained in Section 2, the two hard constraints of topology and safety must be respected. To validate that the output is free of topological errors, the ArcGIS Pro *validate topology* tool, is used. The tool runs a set of integrity checks to identify any topology violations (e.g., overlaps, gaps, self-crossing) as they are defined in the ENC xml file (Nada et al., 2023b).

Regarding safety, the surface-test developed by Kastrisios et al. (2019b) may be used to identify discrepancies between the charted information (i.e., soundings, depth contours, and other features such as rocks and wrecks). However, regarding the requirement that depth contours may only be generalized toward the deep-water side and that small shallows may not be eliminated, no automated validation process exists. Considering that, generally, the readily available generalization tools in ArcGIS Pro are not intended to respect the nautical safety constraints, a validation tool was developed in the Model-builder. The tool detects the safety violations in the output GDB (meaning the sections of the generalized contour/depth area that have been moved on the shallow water side of the source contour/depth area), sort them by the area of the violation (i.e., the size of the polygon formed by the pre and post-generalized contour/depth area), with the aim to highlight the errors for user fixing. The tool is composed of three main stages as shown in Figure 9.

6.1.1 Calculate Difference Polygons

After running the ANG model, the pre-generalization GDB (input GDB) and the post-generalization (output GDB) are loaded to the safety validation tool, then the tool runs a series of operations as follows:

1. Select depth areas DEPAREs from both GDBs using the NIS FC Subtype (i.e., DepthA).

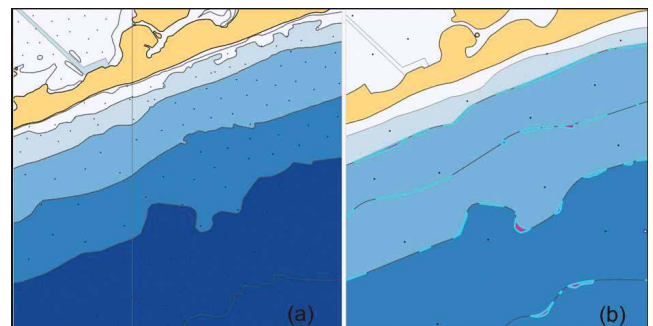


Figure 11. Safety Validation second stage results – safety violations (one feature)

2. Merge Pre & Post generalization DEPAREs into a new single output dataset. All features remain intact even if they overlap (Esri, 2022).
3. Dissolve Pre & Post generalization DEPARE polygons based on specified attributes, for instance Depth Range Value 1 (DRVAL1).
4. Find overlapping areas in the dissolved polygons
5. Split overlapping polygons using the pre-generalized DEPCNT as the cutting features.

The result of this step is a set of polygons that represent the differences between the pre and post-generalized DEPAREs including both the shallow and deep sides (see Figure 10).

The model runs in five main automated phases, utilized by a generalization rule spreadsheet GRS. The spreadsheet is generated from the nautical constraint template, and the input database schema to manage the process and drives data generalization for any desired output scale

6.1.2 Separate Deep vs Shallow Side Polygons

The second stage in the safety validation tool is to separate the results from stage-1 into shallow and deep generalized polygons, in other words safe and unsafe generalization.

As illustrated in Figure 9, after selecting DEPAREs from both pre- and post-generalization GDBs, stage-2 runs as follows:

1. Union pre and post generalization DEPAREs.
2. Delete the overlapping polygons with land areas resulted from generalization.
3. Select Overlaps where DRVAL1 of DEPARE1 = DRVAL2 of DEPARE2.

The result of this stage is all the safety violation polygons but as one feature (Figure 11).

6.1.3 Detect Safety Violation Polygons

As illustrated in Figure 12, the final stage in the validation tool is simply to split the safety violation polygons from stage-2 then sort them by area as follows:

1. Merge polygons from stage-1 and stage-2.
2. Dissolve polygons.
3. Find Overlaps.
4. Sort by area.

The output of this stage (Figure 12 c, d) is the safety violation polygons sorted in a geo-table by area and perimeter. Accordingly, as a user perception, small and irrelevant violation polygons can be accepted according to scale requirements, this is mainly due to the fact that the highest level of detail information is available in the larger scale chart below. In other words, when the mariner zooms in, all the needed information will be available in the larger scale ENC.

7. Conclusion

This paper presented an Automated Nautical-chart Generalization (ANG) model as well as a contours' safety validation tool. The ANG model, aims to describe and implement the steps for generalizing large scale ENC data to the target smaller scale. The model is developed in ArcGIS Pro and runs in five main automated phases, utilized by a generalization rule spreadsheet GRS. The spreadsheet is generated from the nautical constraint template, and the input database schema to manage the process and drives data generalization for any desired output scale. The model output was tested in different areas, with different scenarios, and validated for the mandatory validation checks and nautical hard constraints of topology and safety. The ArcGIS topology validation tool confirms that the output is free of topology errors. However, since the available with ArcPro tools are not generally designed to respect safety, violations are expected / encountered in terms of both soundings and depth

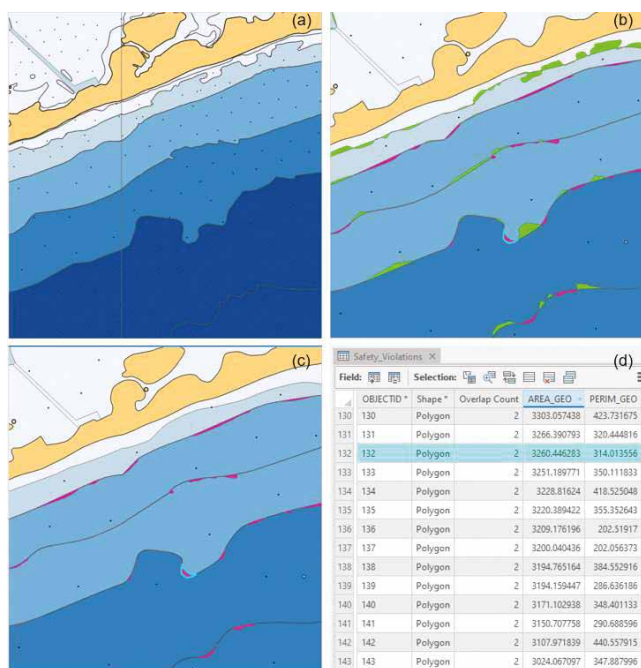


Figure 12. Safety Validation tool results (a) Input GDB (b) Output GDB with safe generalization-green and unsafe-red (c) Safety violations polygons (separated) (d) Geo-table with safety violations area and perimeter

contours/depth areas generalization. Therefore, a safety validation tool was developed and presented that is capable of detecting the safety violations in the model output through three main stages, sort it by area and highlight them for user fixing.

8. Acknowledgements

The work of Tamer Nada, Christos Kastrisios and Brian Calder was supported by the National Oceanic and Atmospheric Administration under grant number NA20NOS4000196.

9. References

- Alexander L. (2003). "Electronic Charts." In *The American Practical Navigator*. 199–215 Bethesda, MD: National Imaging and Mapping Agency.
- Dias T., Monteiro C., Moura A., David J., Cabral P., and Campos F.S., (2022). "Detection of discrepancies between nautical charts and new survey data using GIS techniques". *Cartography and Geographic Information Science*, DOI: 10.1080/15230406.2022.2130823
- Dyer N., Kastrisios, C., and De Floriani, L. (2022). "Label-Based Generalization of Bathymetry Data for Hydrographic Sounding Selection". *Cartography and Geographic Information* 1-16. <https://doi.org/10.1080/15230406.2021.2014974>.
- Ence C. (2018). "Developing Rasterization Procedure for Vector Chart Data". University of Maryland – GEOG 797, Spring 2018.
- Esri (2021). "Getting Started with Topographic Production Generalization". Topographic generalization model documentation by ESRI.
- Esri (2022). "ArcGIS Production Mapping – Automated Generalization" (Online). Available: <https://www.esri.com/en-us/arcgis/products/arcgis-production-mapping/overview#automated-generalization>
- Guilbert E., Lin H. (2006). "B-Spline curve smoothing under position constraints for line generalization", 14th ACM International Symposium on Geographic Information Systems, ACM-GIS 2006, November 10-11, Arlington, Virginia, USA.
- Guilbert E. and Zhang X. (2012). "Generalization of Submarine Features on Nautical Charts". XXII ISPRS Congress, 25 August – 01 September 2012, Melbourne, Australia.
- Huo X., Zhou C., Xu Y. and Li M. (2022). "A methodology for balancing the preservation of area, shape, and topological properties in polygon-to-raster conversion". *Cartography and Geographic Information Science*, volume 49, 2022.
- IC-ENC. (2022). "IC-ENC S-57 Catalogue", (Online). Available: <https://www.ic-enc.org/our-coverage>
- IHO. (2018). "ENC Validation Checks" (S-58), Ed 6.1.0. Monaco: International Hydrographic Organization.
- IHO. (2020). "ENC Product Specification" (S-57 Appendix B.1-Annex A: Use of Object Catalogue for ENC), Ed 4.2.0. Monaco: International Hydrographic Organization.
- IHO. (2021). "Roadmap for the S-100 Implementation Decade (2020 – 2030)", Annex 3, WEND-100 Principles, December 2021.
- Kastrisios C. and Pilikou M. (2017). "Nautical Cartography Competences and their Effect to the Realization of a Worldwide Official ENC Database, the Performance of ECDIS and the Fulfilment of IMO Chart Carriage Requirement." *Marine Policy* 75: 29–40. DOI: 10.1016/j.marpol.2016.10.007
- Kastrisios C., and Calder B. (2018). "Algorithmic implementation of the triangle test for the validation of charted soundings". *Proceedings of the 7th International Conference on Cartography and GIS*, Sozopol, Bulgaria, June, Bulgarian Cartographic Association. (pp. 18–23). <https://doi.org/10.13140/RG.2.2.12745.39528>
- Kastrisios C., Calder B., Masetti G., and Holmberg P. (2019a). "On the effective validation of charted soundings and depth curves". 2019 US Hydro Conference, 19-21 March 2019, Biloxi, MS, USA.
- Kastrisios C., Calder B., Masetti G. and Holmberg P. (2019b). "Towards Automated Validation of Charted Soundings: Existing Tests and Limitations". *Geospatial Information Science*.
- Kastrisios C., Calder B. and Bartlett M. (2020). "Inspection and Error Remediation of Bathymetric Relationship of Adjoining Geo-objects in Electronic Navigation Charts". Vol.1 8th International Conference on Cartography and GIS. Nessebar, Bulgaria.
- Miao D. and Calder B. (2013). "Gradual Generalization of Nautical Chart Contours with a Cubic B-spline Snake Model". *IEEE Oceans*.863.
- Nada T., Kastrisios C., Calder B., Christie E., Greene C., Bethell A., and Hosuru M. (2022). "The Nautical Cartographic Constraints and an Automated Generalization Model". *Canadian Hydrographic Conference 2022*. Ottawa, Canada.
- Nada T., Kastrisios C., Calder B. R., Christie E., Greene C., and Bethell A. (2023). "An Automated Nautical Chart Generalization Model", *US Hydro Conference 2023*. Mobile, AL, USA.
- Nada T., Kastrisios C., Calder B., Ence C., Greene C. and Bethell A. (2023b). "Towards Automated Compilation of Electronic Navigational Charts: Automated Nautical Generalization Model". *Cartography and Geographic Information Science* (manuscript in preparation).
- NOAA (2019). "Transforming the NOAA ENC -Implementing the National Charting Plan", November 7, 2019.

Govt to complete GIS mapping of entire highway network

The government of India plans to complete the GIS mapping of all national highways, including marking the jurisdictions of all state- owned developers, for better planning, execution and monitoring of the road network and timely completion of projects.

As part of the exercise, the ministry of road transport and highways (MoRTH) has asked all project implementing units of the National Highways Authority of India (NHAI), Border Roads Organization (BRO), National Highways and Infrastructure Development Corporation Ltd (NHIDCL) and the ministry itself to complete marking their jurisdictions of the national highways dashboard before the end of May so that the complete GIS data of highways along with jurisdictional segregation is available for future reference and fast-tracking work.

The main objective of this standard operating procedure (SOP) is to streamline GIS-based data collection for all National Highways in India under the MoRTH. According to a MoRTH office memorandum, the SOP aims to clearly define the responsibility area for each National Highway, utilize a GIS-based mapping system through the media portal for defining networks and data visualisation, implement a verification process by the administrative team to ensure data accuracy and reliability and use the collected data for various communication purposes related to the highway system.

Tasked to take up highway construction to 50 km per day GIS technology is also expected to come to the aid of road constructing agencies as it would provide proper information on alignments and any obstruction in the path of highways.

Bhaskaracharya National Institute for Space Applications and Geo-informatics (BISAG-N) in Gandhinagar has done the GIS mapping for large portions of NHs and this data has been updated and verified by field units of the different agencies for the ministry. With the marking of jurisdiction of agencies, the process of GIS mapping would be complete, allowing work in new highway alignments to be started at a faster pace.

MoRTH has decided to upload entire NH network on a single unified platform irrespective of the executing agency, be it NHAI, NHIDCL, BRO or state governments to avoid duplication. www.livemint.com

NOAA. (2022), Status of New NOAA ENC's, (Online). Available: <https://distribution.charts.noaa.gov/ENC/rescheme/>

Peters R., Ledoux H. and Meijers M. (2014). "A Voronoi- based approach to generating depth- contours for hydrographic charts", *Marine Geodesy*, 37:2, 145-166.

Skopeliti A., Stamou L., Tsoulos L., & Pe'eri S. (2020). "Generalization of Soundings across Scales: From DTM to Harbour and Approach Nautical Charts". *ISPRS International Journal of Geo- Information*, 9(11), 11. <https://doi.org/10.3390/ijgi9110693>.

Skopeliti A., , Tsoulos L., and Pe'eri S. (2021). "Depth Contours and Coastline Generalization for Harbour and Approach Nautical Charts". *ISPRS International Journal of Geo- Information* 10, <https://doi.org/10.3390/ijgi10040197>

Socha W. and Stoter J.E. (2013), "First Attempts to automatize generalization of Electronic Navigational Charts – Specifying requirements and methods". 16th ICA Workshop on Generalization and Map Production, Dresden, Germany, 23-24 August, 2013.

Sui H., Zhu X. and Zhang A. (2005). "A System for Fast Cartographic Sounding Selection". *Marine Geodesy*, 28 :2, pp. 159-165.

Tsoulos L. and Stefanakis K. (1997). "Sounding selection for nautical charts: An expert system approach". Paper presented at 18th International Cartographic Conference, June 23–27, Stockholm, Sweden.

Owens E. and Brennan R. (2012). "Methods to Influence Precise

Automated Sounding Selection via Sounding Attribution & Depth Areas". Canadian Hydrographic Conference Niagara Falls, Canada, 15-17 May 2012.

Wilson M., Masetti G., and Calder B. (2017). "Automated Tools to Improve the Ping-to-Chart Workflow," *International Hydrographic Review*, vol. 17, pp. 21-30, May 2017.

Yan J., Guilbert E. and Saux. E. (2017). "An ontology- driven multi-agent system for nautical chart generalization". *Cartography and Geographic Information Science*, 44:3.

Yu W. (2018). "Automatic Sounding Generalization in Nautical Chart Considering Bathymetry Complexity Variations", *Marine Geodesy*, 41:1, pp. 68-85.

Nautical Chart Considering Bathymetry Complexity Variations", *Marine Geodesy*, 41:1, pp. 68-85. sounding selection". *The International Hydrographic Review*, 69(1).

Zhang X. and Guilbert E. (2011). "A multi-agent system approach for feature-driven generalization of isobathymetric line". In Ruas A, editor, *Advances in Cartography and GIScience*. Volume 1, pages 477–495. Springer.

© Author(s) 2023. CC BY 4.0 License.

The paper was first published in the Proceedings of the International Cartographic Association, 5, 14, 2023.

31st International Cartographic Conference (ICC 2023), 13–18 August 2023, Cape Town, South Africa.

The paper is republished with authors' permission. ▴

GNSS Constellation Specific Monthly Analysis Summary: April 2024

The analysis performed in this report is solely his work and own opinion. State Program: U.S.A (G); EU (E); China (C) "Only MEO- SECM satellites"; Russia (R); Japan (J); India (I)



Narayan Dhital

Actively involved to support international collaboration in GNSS-related activities. He has regularly supported and contributed to different workshops of the International Committee on GNSS (ICG), and the United Nations Office for Outer Space Affairs (UNOOSA). As a professional employee, the author is working as GNSS expert at the Galileo Control Center, DLR GfR mbH, Germany.

Introduction

The article is a continuation of monthly performance analysis of the GNSS constellation. In this month’s issue, there is an additional monitoring of the satellite Timing Group Delay (TGD)/ Broadcast Group Delay (BGD) parameters in terms of their applicabilities.

Analyzed Parameters for March, 2024

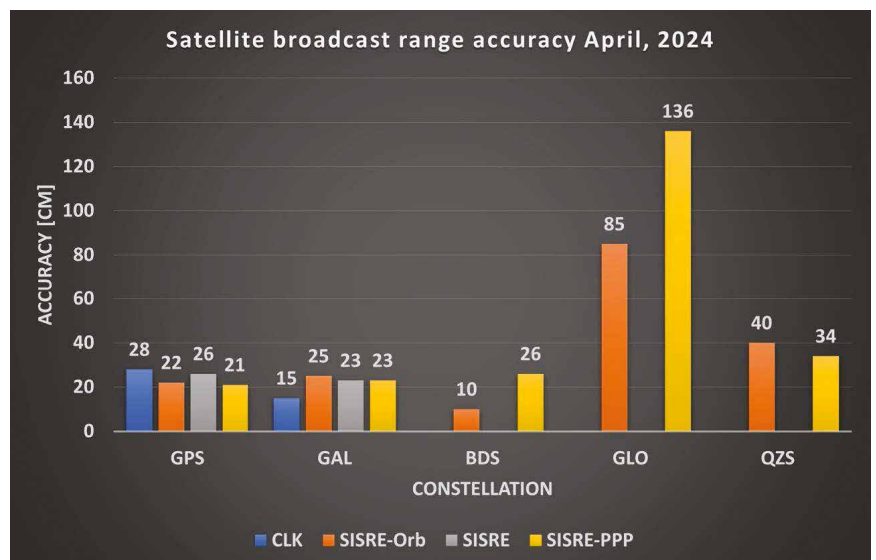
(Dhital et. al, 2024) provides a brief overview of the necessity and applicability of monitoring the satellite clock and orbit parameters.

- a. Satellite Broadcast Accuracy, measured in terms of **Signal-In-**

Space Range Error (SISRE) (Montenbruck et. al, 2010).

- b. **SISRE-Orbit** (only orbit impact on the range error), SISRE (both orbit and clock impact), and **SISRE-PPP** (as seen by the users of carrier phase signals, where the ambiguities absorb the unmodelled biases related to satellite clock and orbit estimations. Satellite specific clock bias is removed) (Hauschlid et.al, 2020)
- c. **Clock Discontinuity:** The jump in the satellite clock offset between two consecutive batches of data uploads from the ground mission segment. It is indicative of the quality of the satellite atomic clock and associated clock model.
- d. **URA:** User Range

(a), (b) Satellite Clock and Orbit Accuracy (monthly RMS values)



Accuracy as an indicator of the confidence on the accuracy of satellite ephemeris. It is mostly used in the integrity computation of RAIM.

- e. **GNSS-UTC offset:** It shows stability of the timekeeping of each constellation w.r.t the UTC
- f. **Satellite Hardware Delay (TGD/BGD):** The hardware delays originating from the analog and digital parts of the satellite’s transmission. Mostly, the time difference between the transmitted RF signal, measured at the transmitting antenna, and the signal at the output of the onboard frequency source.

Note:- for India’s IRNSS there are no precise satellite clocks and orbits as they broadcast only 1 frequency which does not allow the dual frequency combination required in precise clock and orbit estimation; as such, only URA and Clock Discontinuity is analyzed.

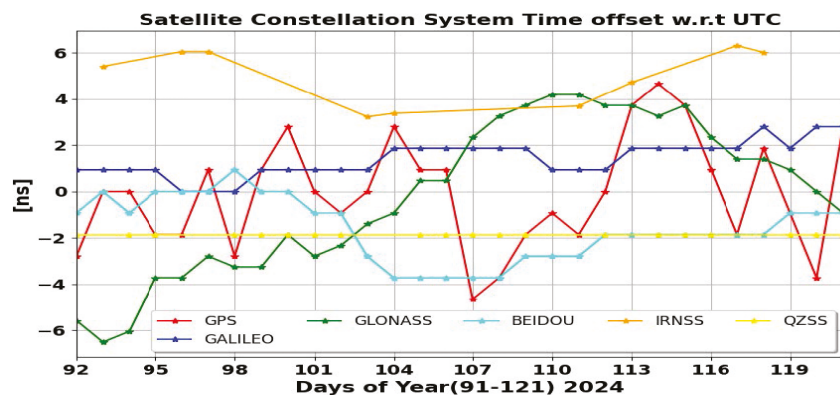
(c) Satellite Clock Jump per Mission Segment Upload

Const	Mean [ns]	Max [ns]	95_Percentile [ns]	99_Percentile [ns]	Remark (Best and Worst 95 %)
IRNSS	3.86	1306.33	6.39	23.31	Best I03 (3.57 ns) Worst I06 (12.96 ns) I10 had large jumps on multiple occasions; I02 had several moderate jumps
GPS	16.15	552184.37	0.43	2.55	Best G04 (0.41 ns) Worst G03 (2.44 ns) G21 (frequent jumps from day 108 to 115-also observed in SISRE-CLK analysis), G17 (non-healthy/unusable, large jumps on day 094-095)
GAL	0.09	3.35	0.19	0.44	Best E07 (0.15 ns) Worst E19 (0.33 ns)

(d) User Range Accuracy (Number of Occurrences in Broadcast Data 01–30 April)

IRNSS-SAT	2 [m]	2.8 [m]	4.0 [m]	5.7 [m]	8 [m]	8192 [m]	9999.9 [m]	Remark Other URA values (frequency)
I02	2852	12	6	-	1	1	3	-
I03	521	6	4	-	1	-	-	-
I06	706	3	1	1	6	-	3	URAs 16 (1), 32 (1) 64 (1), 128 (1)
I09	412	3	-	-	1	1	-	URAs 16(1)
I10	733	5	-	-	1	-	-	-

(e) GNSS-UTC Offset



(f): Satellite Hardware Delay (TGD/BGD and Precise DCB)

(Dhital et.al, 2024) discussed briefly on the TGD/BGD parameters transmitted by the GNSS satellites. In this month’s issue, the compatibility of such parameters with the post-processed and highly precise Differential Code Bias (DCB) products is discussed. The one-to-one comparison of TGD/BGD and DCB values does not make much sense as different conventions are used in the respective estimation of broadcast values and post-processed DCB. In the network processing, the functional model of GNSS observations suffers from a singularity as unique solution to the estimable parameter is not available. As explained in (Montenbruck et.al, 2014 a), the clock offset parameters and code bias parameters cannot be uniquely estimated in the same estimation process. However, when two signals are combined to the same satellite and receiver pair, the clock offset parameters can be removed. Following this approach, the estimation of satellite plus receiver biases for all network stations and satellites is possible. The next step is to separate the satellite code bias and receiver code bias.

$$X^{Sat} = (DCB^{Sat,1}, \dots, DCB^{Sat,n})^T$$

$$X^{Rec} = (DCB^{Rec,1}, \dots, DCB^{Rec,m})^T$$

Here, if z is considered to denote the vector of k observed DCBs (combination of Satellite and Station DCBs denoted by X^{Sat} and X^{Rec}), then the resulting system of equation is formulated as $z = AX^{Sat} + BX^{Rec}$, for which least square estimation can be used. The normal equation used to solve the problem exhibits a rank deficiency since a bias common to all satellites cannot be distinguished from a corresponding bias common to all receivers. In other words, if a constant is added to all satellite bias in the observation model, then the same constant can be added to all the receiver bias, to keep the observed value unchanged. Therefore, for a realistic estimation of satellite biases a constraint needs to be imposed on the equations of least square estimation which removes the rank-deficiency/singularity. There are

different ways to apply the constraint, but commonly used approaches are to fix one calibrated receiver (mostly used in control segment of the GNSS) and to impose constellation zero-mean condition (as used in post-processed precise bias estimation). This also means the estimated satellite biases are relative to the used constraint, which is very important to consider while analyzing the TGD and DCB values. If zero-mean constellation condition is used

$$\sum_{i=1}^n DCB^{SAT,i} = 0$$

With this approach, an attention must be paid in the event of status change in the constellation (i.e., removal/addition of satellites) as this renders a systematic offset. This effect is monitored for Galileo constellation as shown in Figure f (a). However, the linear dependencies of bias and clock offset parameters renders no impact in the positioning solution as the receiver clock offset absorbs such systematic offset common to all satellites. For the analysis shown in the subsequent plots, the precise products from Chinese Academy of Sciences (CAS) are used for the comparison and days of year between 021 and 121, 2024 are taken. Note that, CAS DCB products are not available in the ftp for days 001 to 020 and day 085.

As both broadcast BGD and CAS precise DCB for Galileo are referenced to the zero-mean constellation constraint, a direct comparison shall also suffice. But the objective here is to validate the above-mentioned conventions with the data. As such, both broadcast BGD and CAS DCB are realigned towards the zero-mean constellation constraint (the daily mean of constellation is removed from individual satellite). It is clear from Figure f (a)(bias without alignment to the convention) that Galileo broadcast BGD has a systematic offset after day of year around 72 w.r.t the precise DCB. What this means is that there was a potential change in the satellites used in the Galileo mission control segment procedures. As per Galileo

constellation status (i.e., NAGU), Galileo SAT GSAT0104 was decommissioned from around that time. When analyzed separately (not shown in Figure), the

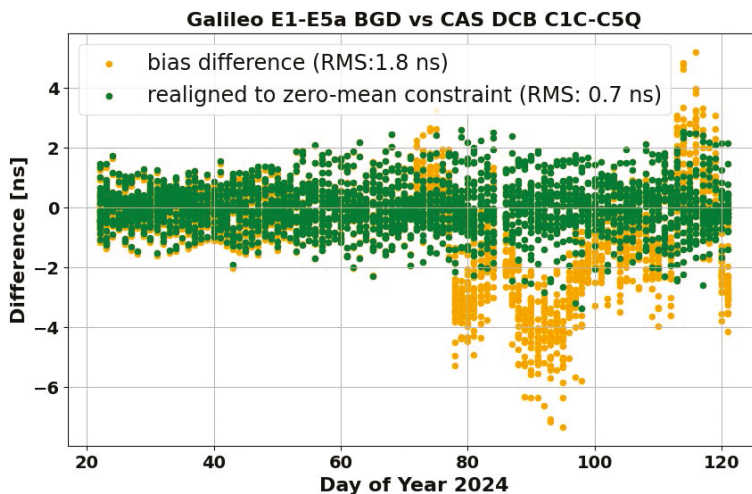


Figure f a: The comparison of broadcast BGD for Galileo E1-E5a w.r.t CAS final DCB C1C-C5Q.

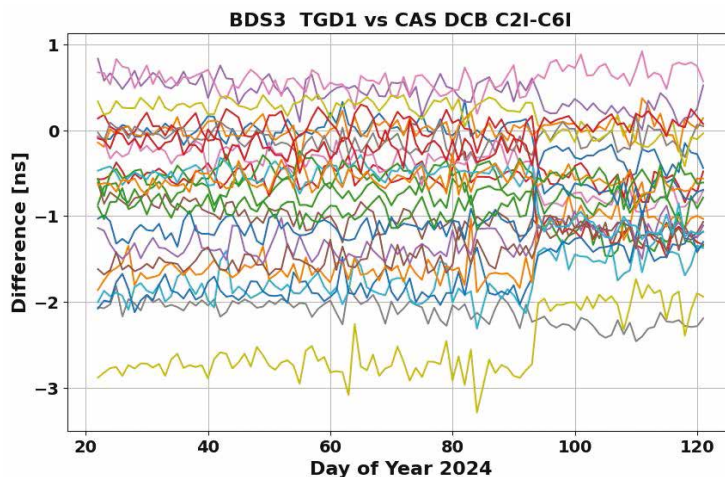


Figure f b: The comparison of Beidou 3 TGD1 w.r.t CAS final DCB C2I-C6I. Each color indicates individual Beidou 3 satellite.

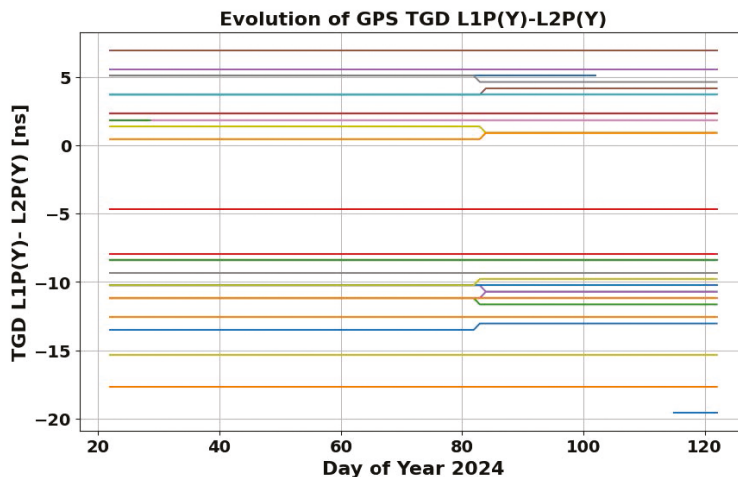


Figure f c: Temporal evolution of TGD values transmitted by GPS. One noticeable shift is detected for PRN 01 (shown as blue line at the bottom of the plot after day of year 113).

CAS DCB products show consistent behavior referenced to zero-mean constellation. In the same Figure f (a), the comparison between BGD and DCB, where both dataset are aligned to the reference constraint, shows better consistencies without any noticeable shifts. The RMS (or the standard deviation in this case as the mean value is removed) is 0.7 ns over the analyzed period.

Similar approach is carried out for Beidou 3 satellites, where the broadcast TGD1 values are realigned to the zero-mean condition of all available Beidou satellites. The result (Figure f (b)) shows RMS value of 1.10 ns over the analyzed period. Due to different calibration strategy used for TGD1 and CAS DCB estimators, this value shows only a rough indication and systematic offsets may still exist.

As for GPS constellation, the noticeable shift of TGD parameter in PRN 1 (blue line, the shifted value after day of year 113 is isolated in the bottom of plot) is observed in Figure f (c). It shows the bias value switches from around 5 ns to around -19 ns. The GPS constellation status (i.e., NAGU advisory number “2024020”) reports that on approximately 22 April (day of year 113) satellite vehicle number SVN49 resumes transmitting L-band in PRN01 and advises not to use PRN01 until further notice. In GPS control segment, calibrated reference receivers are used to fix the rank deficiency in network estimation of TGD and this is why only PRN01 has shifted value without impacting other satellites. In terms of broadcast BGD/TGD, there are no other significant jumps/shift in all GNSS satellites for the month of April. For recap, the values for TGD/BGD are either calibrated and uploaded to the satellite or estimated as a part of the mission control activities and then uploaded to the satellite with varying temporal resolutions (Wang et.al, 2019). This indicates the TGD/BGD values are slowly varying.

There as an additional step not explained above which relates to the frequency scaling factors for the respective DCB signal combinations. As the broadcast satellite clock offset is referenced to the linear combination of signals, single frequency observational model shall consider the DCB parameter in the model. Otherwise, the satellite clock inconsistency will propagate into the positioning solution. Similar consideration is needed if TGD is used instead of DCB (which is available with larger latency) in the single frequency modeling. When comparing these two approaches (Guo et.al, 2015), the relationship between TGD and DCB can be derived as:

$$TGD = \frac{1}{1-\gamma} DCB(f1, f2)$$

Here, the frequency scaling factor for two signals with frequencies f1 and f2 is: $\gamma = \frac{f_1^2}{f_2^2}$

Monthly Performance Remarks:

1. Satellite Clock and Orbit Accuracy:
 - For GPS, the satellite clock and orbit accuracy shows similar performance as in March 2024. There were couple of satellite outages and NANU and removed from the analysis. GPS PRN 17 had an unusable status on day of year 094 and 095. G01 is removed completely in the analysis. G21 had moderately large clock errors from day 108 to 115. It was included in the analysis.
 - For Galileo, all parameters showed consistent performances.
 - For GLONASS, the performance looked similar to the past months. Satellite R07 seemed maneuvering from day 106 to day 111 bad orbit on day 106. Satellites R09 and R11 have slightly degraded orbits from day 113 to 121.
 - For BDS and QZSS, the performance looks very much the same as in the past. For QZSS, there are days with better orbit quality and some days with degraded performance. On day 121, QZSS J02 had a very large satellite clock offset jump.

- For IRNSS, the notable difference in this month’s performance is the inconsistent URA for I06 satellite. There were a varying confidences in the range accuracy for I06.
2. UTC Prediction (GNSS-UTC): Galileo constellation is more stable within 2.5 ns in the GNSS-UTC prediction. In March, 2024, the values ranged from 1 ns to 9 ns.

References

- Cao X, Zhang S, Kuang K, Liu T (2018) The impact of eclipsing GNSS satellites on the precise point positioning, Remote Sensing 10(1):94
- Dhital N (2024) GNSS constellation specific monthly analysis summary, Coordinates, Vol XX, Issue 1, 2, 3, 4
- Hauschlid A, Montenbruck O (2020) Precise real-time navigation of LEO satellites using GNSS broadcast ephemerides, ION
- Guo F, Zhang X, Wang J (2015) Timing group delay and differential code bias corrections for BeiDou positioning, J Geod,
- IERS C04 (2024) <https://hpiers.obspm.fr/iers/eop/eopc04/eopc04.1962-now>
- IGS (2021) RINEX Version 4.00 https://files.igs.org/pub/data/format/rinex_4.00.pdf
- Li M, Wang Y, Li W (2023) performance evaluation of real-time orbit determination for LUTAN-01B satellite using broadcast earth orientation parameters and multi-GNSS combination, GPS Solutions, Vol 28, article number 52
- Li W, Chen G (2023) Evaluation of GPS and BDS-3 broadcast earth rotation parameters: a contribution to the ephemeris rotation error Montenbruck O, Steigenberger P, Hauschlid A (2014) Broadcast versus

precise ephemerides: a multi-GNSS perspective, GPS Solutions

Liu T, Chen H, Jiang Weiping (2022) Assessing the exchanging satellite attitude quaternions from CNES/CLS and their application in the deep eclipse season, GPS Solutions 26(1)

Montenbruck O, Steigenberger P, Hauschlid A (2014) Broadcast versus precise ephemerides: a multi-GNSS perspective, GPS Solutions

Montenbruck O, Hauschlid A (2014) a) Differential Code Bias Estimation using Multi-GNSS Observations and Global Ionosphere Maps, ION

Steigenberger P, Montenbruck O, Bradke M, Ramatschi M (2022) Evaluation of earth rotation parameters from modernized GNSS navigation messages, GPS Solutions 26(2)

Sylvain L, Banville S, Geng J, Strasser S (2021) Exchanging satellite attitude quaternions for improved GNSS data processing consistency, Vol 68, Issue 6, pages 2441-2452

Wang N, Li Z, Montenbruck O, Tang C (2019) Quality assessment of GPS, Galileo and BeiDou-2/3 satellite broadcast group delays, Advances in Space Research

Data sources:

<https://cddis.nasa.gov> (Daily BRDC); <http://ftp.aiub.unibe.ch/> (CODE_MGEX/CODE/ (Precise Products); BKG “SSRC00BKG” stream; IERS C04 ERP files

(The monitoring is based on following signals- GPS: LNAV, GAL: FNAV, BDS: CNAV-1, QZSS:LNAV IRNSS:LNAV GLO:LNAV (FDMA)) 

NEWS - GNSS

Two new satellites join the Galileo constellation

The European Galileo navigation system has two more satellites in orbit following their launch on a SpaceX Falcon 9 on 28 April. With 30 satellites now in orbit, Galileo is expanding its constellation.

Since the conception of Galileo, 38 Galileo satellites have been developed and tested by ESA and European industry for the EU’s Galileo programme. Of these, four In-Orbit-Validation and 26 Full Operation Capability satellites have been placed in orbit with 12 launches.

The launch took place only a few days after the new Public Regulated Service (PRS) signals started to be broadcasted. This encrypted navigation service is specifically designed for authorised governmental users and sensitive applications, contributing to increase Europe’s autonomy and resilience in the critical domain of satellite navigation. www.esa.int

Finnair cancels flights amid increased GNSS jamming

Finnair, the sole international airline operating flights to Tartu, Estonia, has suspended its daily service to the city from April 29 to May 31, 2024. The decision comes in response to ongoing GNSS interferences and disruptions, including two instances where flights had to return to Helsinki, Finland, due to excessive jamming in the region.

The current approach methods at Tartu Airport rely heavily on GNSS signals, which have been disrupted frequently in the area. To address this, Finnair plans to use the one-month flight suspension period to develop and implement alternative navigation methods at Tartu Airport that can operate independently of GNSS. Finnair aims to enhance the safety and reliability of operations, preventing similar incidents in the future.

This suspension of flights highlights a broader issue of increasing GNSS jamming and spoofing, which has been a

growing concern since the start of the Ukraine war in 2022 — specifically near Kaliningrad, the Black Sea, the Caspian Sea and the Eastern Mediterranean.

UK government tests quantum-inertial navigation technology

The UK has successfully completed commercial flight trials of advanced quantum-based navigation systems that cannot be jammed or spoofed by hostile actors.

While GPS jamming is currently relatively rare and does not directly impact an aircraft’s flight path, new quantum-based Positioning, Navigation, and Timing (PNT) systems could, over time, offer one part of a larger solution to providing highly accurate and resilient navigation that complements current satellite systems – which could help ensure that the thousands of flights that take place around the world daily, proceed without disruption.

Infleqtion, a quantum technology firm, in collaboration with aerospace companies BAE Systems and QinetiQ, completed the trials at MoD Boscombe Down in Wiltshire, with Science Minister Andrew Griffith aboard the final test flight on Thursday 9 May. These tests are the first time that this sort of ground-breaking technology has been tested in the UK on an aircraft in flight, and the first such flights worldwide have been publicly acknowledged. www.infleqtion.com

ComNav rolls out Survey Master 3.5.0

ComNav Technology Ltd. has released the latest version of the Survey Master software - Survey Master 3.5.0. This update focuses on addressing long-standing core issues for users, introducing a series of innovative features and enhancements. From this version onwards, users use ComNav controllers can automatically receive permanent registration rights to the software, accessing all features without the need for additional registration codes. www.comnavtech.com 

WILDetect: An intelligent platform to perform airborne wildlife census automatically in the marine ecosystem

A new non-parametric approach, WILDetect, has been built using an ensemble of supervised Machine Learning (ML) and Reinforcement Learning (RL) techniques. We present here the first part of the paper. The concluding part will be published in next month



Kaya Kuru

Corresponding author
School of Engineering,
University of Central
Lancashire, Fylde Rd,
Preston, Lancashire,
PR12HE, UK



Stuart Clough

APEM Inc., 2603 NW 13th
Street, 402, Gainesville,
FL 32609-2835, USA¹



Darren Ansell

School of Engineering,
University of Central
Lancashire, Fylde Rd,
Preston, Lancashire,
PR12HE, UK



John McCarthy

APEM Ltd., The
Embankment Business
Park, Stockport,
SK4 3GN, UK²



Stephanie McGovern

APEM Ltd., The
Embankment Business
Park, Stockport,
SK4 3GN, UK

Abstract

The habitats of marine life, characteristics of species, and the diverse mix of maritime industries around these habitats are of interest to many researchers, authorities, and policymakers whose aim is to conserve the earth's biological diversity in an ecologically sustainable manner while being in line with indispensable industrial developments. Automated detection, locating, and monitoring of marine life along with the industry around the habitats of this ecosystem may be helpful to (i) reveal current impacts, (ii) model future possible ecological trends, and (iii) determine required policies which would lead accordingly to a reduced ecological footprint and increased sustainability. New automatic techniques are required to observe this large environment efficiently. Within this context, this study aims to develop a novel platform to monitor marine ecosystems and perform bio census in an automated manner, particularly for birds in regional aerial surveys since birds are a good indicator of overall ecological health. In this manner, a new non-parametric approach, WILDetect, has been built using an ensemble of supervised Machine Learning (ML) and Reinforcement Learning (RL) techniques. It employs several hybrid techniques to segment, split and count maritime species – in particular, birds – in order to perform automated censuses in a highly dynamic marine ecosystem. The efficacy of the proposed approach is

demonstrated by experiments performed on 26 surveys which include Northern gannets (*Morus bassanus*) by utilising retrospective data analysis techniques. With this platform, by combining multiple techniques, gannets can be detected and split automatically with very high sensitivity (Se) (≈ 0.97), specificity (Sp) (≈ 0.99), and accuracy (Acc) (≈ 0.99) — these values are validated by precision (Pr) (≈ 0.98). Moreover, the evaluation of the system by the APEM staff, which uses a completely new evaluation dataset gathered from recent surveys, shows the viability of the proposed techniques. The experimental results suggest that similar automated data processing techniques – tailored for specific species – can be helpful both in performing time-intensive marine wildlife censuses efficiently and in establishing ecological platforms/models to understand the underlying causes of trends in species populations along with the ecological change.

1. Introduction

The oceans cover two-thirds of the Earth's surface and the maritime economy has always been diverse and abundant. With the applications of emerging fields of science and technology in new and existing industries, prominent companies and research organisations have been recently developing and deploying evolving technologies supported by location-independent advanced maritime

The detection of small objects, particularly birds, in large-scale images with more than 50 million pixels is a non-trivial task when using manual approaches. Long-term data that utilises standardised and structured methodologies are ideal for quantifying change in species populations

mechatronics systems (AMMSs) (Kuru & Yetgin, 2019; Shi et al., 2017) to explore and exploit the resources in this tough landscape. This massively evolving industry, enabling enormous continuous human control in the maritime, has the potential to impact the marine ecosystem dramatically; in particular, the seabed, birds, turtles, and fish. Birds are an inseparable part of the maritime ecosystem. Seabird population changes are good indicators of long-term and large-scale change in marine ecosystems, and important because their populations are strongly influenced by threats (e.g., entanglement in fishing gear, overfishing of food sources, climate change, pollution, disturbance, direct exploitation, development, energy production) to marine and coastal ecosystems (Palczny et al., 2015). Considerable differences in population trajectories of off-shore bird families have been documented, which suggests that overall offshore bird populations are decreasing (BOEM, 2022). The monitored portion of the global seabird population, representing approximately 19% of the global seabird population, has declined by nearly 70% between 1950 and 2010 (Palczny et al., 2015), a net loss approaching 3 billion birds (u.e., %29) since 1970 (Rosenberg et al., 2019). This loss of bird abundance signals an urgent need to address threats to avert future avifaunal collapse and associated loss of ecosystem integrity, function, and services (Rosenberg et al., 2019).

One type of bird is the northern gannet (*Morus bassanus*), the largest seabird in the North Atlantic, having a wingspan of up to 180 cm and a length of up to 100 cm (RSBP, 2015). More specifically, gannets are large white birds with distinctive features including yellowish heads and black-tipped wings. They are distinctively shaped with a long neck and long pointed beak, long pointed tail, and long pointed wings (RSBP, 2015). An example is displayed in Fig. 1. The most important nesting



Fig. 1. Example of a gannet in a high-resolution image.³

ground for northern gannets is the UK with about half of the world's population (55.6%) (JNCC, 2015). APEM Ltd⁴ has a wide range of gannet data with geographical positions obtained from all around the world and this species is the focus of this study which aims to test the developed approaches to help perform further autonomous bird censuses paving the way for automated classification of multispecies and counting them. The censuses of gannets have been undertaken since the 1980s (JNCC, 2015; Murray et al., 2015) and all Scottish colonies were surveyed in 2013 and 2014 via manual approaches (Murray, Harris et al., 2014; Murray et al., 2015; Murray, Smith et al., 2014). In a typical marine survey programme, there might be around half a million images taken over 12 months for a specific area and it is a labour-intensive task to separate this survey into positive images with targeted objects and negative images with no objects, and then count the objects in the images deemed positive. Many surveys acquired by APEM Ltd suggest that more than 95% of the images contain no targeted objects. The detection of small objects, particularly birds, in large-scale images with more than 50 million pixels is a non-trivial task when using manual approaches. Long-term data that utilises standardised and structured methodologies are ideal for quantifying change in species populations; Unfortunately, such data does not exist for most biogeographic regions (Clements & Robinson, 2022) due to the difficulties and high cost of manual methods. Therefore, automation of this work using an automated intelligent computer system which would help the development of effective prospective environmental models with realistic inputs is highly beneficial.

Despite recent advances in computer vision and learning techniques as well as many attempts to monitor off-shore species in an automated manner, comprehensive large off-shore wildlife censuses are still conducted manually by experienced ecologists, ethologists, ornithologists (e.g., JNCC, 2022; Thompson, 2021) due to unmet expectations in accuracy rates for the counting and classification of species via automated methods as elaborated in Sections 2, 3 and 4.1. With this motivation in mind considering the challenges mentioned in Section 3, this study proposes a new supervised Machine Learning (ML) approach supported by Reinforcement Learning (RL) enabling user-model-data interaction that can detect, split and count birds, in particular, offshore gannets, in an automated decision-making way with high accuracy rates. To clarify the novelty of this paper, particular contributions are outlined as follows.

1. This is the first attempt that explicitly aims to implement maritime bio censuses in marine surveys automatically

using an ensemble of supervised ML and RL techniques with a user model-data interaction in finding the best analysis parameters for mitigating the highly dynamic characteristics of the maritime ecosystem.

2. The two phases of using ensemble techniques within the developed methodology can work successfully in performing the offshore bird censuses and most importantly, the methodology can be generalised to the automated classification and counting of broader maritime multispecies. The methodology can be expandable with more feature extraction techniques in addition to the employed three techniques to achieve higher accuracy rates.
3. The proposed approach shows a new direction for the detection of particular, small species with a diverse background and most importantly for the classification of multispecies even if there is a strong resemblance between them, as seen in bird species, where current techniques (i.e., off-the-shelf approaches (e.g., OBIA), Deep Neural Network (DNN) (e.g., CNN)) cannot converge to a desired solution with high accuracy rates based on the features of datasets.

The remainder of this paper is organised as follows.

Section 2 surveys the related literature. Section 4 reveals how the methodology is built up. The implementation of the established methodology in splitting and counting the particular species in surveys is explained in Section 5. The results are presented in Section 6. Discussions are provided in Section 7. Finally, Section 8 draws conclusions and provides directions for potential future ideas.

2. Literature review

Wang et al. (2019) reviews studies regarding wild animal surveys based on multiple platforms, including satellites, manned aircraft, and unmanned aircraft systems (UASs), and focuses on the data used, animal detection methods, and their accuracies. The resolution of (sub-metre) satellite images is not sufficient to discern small (<0.6 m) animals at the species level; Manned aerial surveys have long been employed to capture the centimetre-scale images (with a spatial resolution of 2.5 cm Hollings et al., 2018) required for animal censuses over large areas whereas UASs can cover only small areas (Wang et al., 2019). Groom et al. (2013) analysed a very limited number of images (18 frames) within two offshore areas in the Irish Sea using an off-the-shelf object-based image analysis (OBIA) algorithm, aiming at combining manual and automated image analysis, to describe marine bird distributions and abundances. Similarly, Chabot et al. (2018) used OBIA to detect and count Lesser Snow Geese in large numbers of images of breeding colonies across the Canadian Arctic, achieving better results compared to human counting. It is noteworthy to mention that the prevalent use of aerial thermal-infrared images for detecting large mammals is of limited applicability to seabirds because of the low pixel resolution of thermal cameras, the smaller size of birds (Chabot & Francis, 2016),

and most importantly their low body temperature. Borowicz et al. (2019) established a semi-automated approach using deep learning networks for whale detection from satellite imagery with sub-metre resolution. Kellenberger et al. (2021) developed an approach to automatically detect and count seabirds in UAS imagery using deep convolutional neural networks (CNNs) resulting in low accuracy rates for some types of species regarding the insufficient number of training species for the CNN technique. Again, Dujon et al. (2021) developed a deep CNN using UAS imagery to detect three types of species, in particular, gannets with an overall precision of 0.74. Hong et al. (2019) employed several types of DNNs in non-marine bird detection, resulting in precision values ranging from 85.01% to 95.44%. Hayes et al. (2021) employed CNN in counting two types of birds on the shore in the sitting state using UAS at a close range, resulting in success rates of 97.66% for Black-browed Albatrosses, and 87.16% for Southern Rockhopper Penguins. Close-range use of UAS may disturb wildlife or disrupt their normal activities (Johnston, 2019), especially for flying birds. Akçay et al. (2020) conducted on-ground flying bird detection on bird population movement trends using several DNN techniques with precision values ranging from 0.86 and 0.94. Alqaysi et al. (2021) found the precision values ranging from 60% to 92% for bird detection around wind farms using DNN. There is no guarantee in achieving good accuracy rates using the most popular learning technique, the so-called DNNs. It can be concluded that these approaches require a huge amount of data samples to achieve a satisfactory training outcome (Delhez, 2022). The aforementioned techniques are discussed in Section 7 considering the proposed approach in this study. It is worth discussing the emerging promising approach, namely, Deep Reinforcement Learning (DRL) here as well. Recent revolutionary advances in artificial intelligence (AI) using the learning principles of biological brains and human cognition has fuelled the development and use of Deep Reinforcement Learning (DRL) in numerous fields such as Atari games (Mnih et al., 2015), poker (Moravčík et al., 2017), multiplayer games (Jaderberg et al., 2019), and board games (Silver et al., 2016; Silver, Hubert et al., 2017; Silver et al., 2018; Silver, Schrittwieser et al., 2017). DRL has surpassed human-level performance in many similar applications. It, with goal-directed behaviour and representation

We have employed an ensemble of ML and RL techniques for automated recognition, splitting, and counting of birds in aerial surveys to both reach our goals in accuracy rates and classify multispecies in the further development of the proposed application

learning with the ability to learn different levels of abstraction from data, has emerged as a very effective approach by combining the strengths of two successful approaches – RL and DNN – to overcome the representation problem of RL as function approximators, which generalises knowledge to new unseen complex situations. More explicitly, DRL can be defined as a function approximation method in DNN to generalise past experiences to new situations in complex scenarios by mapping them to near-optimal decisions using scalable and generalisable optimal policies. DRL, in particular, with the most commonly used Deep Q-Networks (DQN), has been found successful in addressing high dimensional problems with less prior knowledge. However, to the best of our knowledge, DRL has been employed for generalising past experiences to a new situation to find the best optimal decision and has yet to be employed for a problem space similar to the one mentioned in this paper. Therefore, this method seems not applicable to our objectives considering the aforementioned problem space which is defined in Section 3.

3. Problem definition

Very large areas need to be surveyed in shorter time spans to understand the ecological footprint and to take necessary measures accordingly in a timely manner. Despite recent advances in computer vision and learning techniques as well as many attempts to monitor off-shore species in an automated manner, comprehensive large off- shore wildlife censuses are still conducted manually by experienced ecologists, ethologists, ornithologists (e.g., JNCC, 2022; Thompson, 2021) due to unmet expectations in accuracy rates for the counting and classification of multispecies via automated methods. Manual approaches increase the cost of surveying large areas significantly and required regular surveys may not be conducted due to this high cost. New automated computer-based approaches are required to observe large areas efficiently and effectively to meet the desired objectives of the research community. We performed a literature survey analysis (Section 2) and conducted several preliminary experiments using the most commonly used techniques to develop the most appropriate approach that can meet the expectations of the research community. The outcomes of our preliminary tests are elaborated in Section 4.1. To summarise considering the survey analysis and preliminary tests specific to the airborne survey data, (i) template-matching approaches (e.g., SIFT) that requires no prior training are far from being able to realise any objectives desired by the research community due to the indistinct features of very small objects within very complex background, (ii) off-the-shelf computer vision techniques (e.g., OBIA) and off-the-shelf ML techniques that require prior training don't result in high accuracy rates due to the indistinct features of very small objects in very big images, and (iii) DNN (e.g., R-CNN), requiring prior training with a large number of data instances,

Despite recent advances in computer vision and learning techniques as well as many attempts to monitor off-shore species in an automated manner, comprehensive large off- shore wildlife censuses are still conducted manually by experienced ecologists, ethologists, ornithologists

do not converge to a desired solution due to the limited number of instances with the indistinct features of very small objects within a diverse background; Besides, the misclassification of multispecies is high with DNN where data instances in different groups resemble each other too closely as seen in bird species.

The literature, to the best of our knowledge, has a gap that can be filled with the research of computer-automated study analyses of species datasets acquired from the photogrammetry settings which use small aeroplanes to survey very large areas in shorter time spans when compared with other approaches that use static locations, ships or UAS. Due to low accuracy rates in detecting small animals in the marine ecosystem using several off-the-shelf computer vision techniques, off-the-shelf ML techniques, template-matching approaches, and DNN, which is elaborated in Section 4.1 regarding the preliminary experiments with our findings (e.g., the changing and complicated background of the sea, number of data samples in the training set, low- quality images of small species that lack clear features due to them being captured by small aeroplanes with remotely-sensed aerial monitoring photogrammetry settings), we developed a novel approach using an ensemble of ML and RL with a motivation to increase the detection accuracy to reach our target (>0.95) and classify multispecies for the further improvement of the application with multispecies training.

4. Methodology

4.1. Technical background

Repetitive surveying of very large areas for the purpose of observing trends and population fluctuations, which also use human-dependent approaches, may result in huge financial and time costs. Therefore, sampling is commonly employed to census species within representative sample areas using varying sampling strategies and a way of statistical prediction or projection to a whole figure to avoid high costs where the larger the sample of sites, the better the approximation. However, there can be many sampling biases in such datasets like spatial,

taxonomic, or temporal leading to inaccurate inferences: Spatial bias refers to uneven sampling efforts across a region; Taxonomic bias can include over or under-representation of certain species in the dataset; Temporal bias occurs when records are collected in one season only, or more often at certain times of the year (Jayadevan et al., 2022). Sampling may not be extrapolated to a reliable figure, in particular, for rare species, considering the high percentage of negative images in whole surveys (> %95) and uneven density and variance in counts of species from one habitat to another, mostly, related to the habitat associations (e.g., food, breeding, sheltering) leading to poor sampling (i.e., oversampling, undersampling), which may produce misleading inferences. Several studies developed particular approaches to mitigate the effect of biases in surveys. For instance, Smyser et al. (2016) utilised a double-observer survey configuration to quantify and correct the bias caused by the failure of observers in aerial surveys. Monitoring all regions of interest and counting all species of interest is crucial to reach highly reliable outcomes and proper decisions with appropriate interpretations. Aerial surveys are an efficient survey platform, capable of collecting wildlife data rapidly across large spatial extents in short time frames; however, these surveys can yield unreliable data if not carefully executed (Davis et al., 2022). To this end, numerous approaches such as entropy-based information screening method (Li et al., 2021) and normalised double entropy (NDE) (Li et al., 2023) were developed to distinguish bad and redundant image data to increase the quality of sampling.

As an active research direction for decades, object recognition and detection have had increased importance within many fields

such as nature, biometrics, medicine, and robotics. Current clustering algorithms, in which no prior training is performed, on visual datasets, are not successful in grouping similar objects with high rates of accuracy, particularly, for objects with very complex backgrounds (Kuru & Khan, 2018). One of the oldest methods of object recognition is the template-matching approach. It consists of sliding a particular template over the search area (usually an image in which we are trying to locate) and at each position, calculating a distortion or correlation measure that estimates the degree of dissimilarity or similarity between the template and the candidate (Reyes, 2014). Then, the minimum distortion or maximum correlation position (depending on the implementation) is taken to represent the instance of the template into the image under examination. There are various ways of calculating the degree of dissimilarity or similarity, such as the Sum of Absolute Differences (SAD) and the Sum of Squared Differences (SSD). The Normalised Cross-Correlation (NCC) is by far one of the most widely used correlation measures (Stefano et al., 2003; Yang, 2010). Recently, several well-advanced template-matching techniques have been developed to detect objects automatically. These off-the-shelf template-matching techniques are scale-invariant feature transform (SIFT), speeded-up robust features (SURF), features from accelerated segment test (FAST), binary robust independent elementary features (BRIEF), oriented FAST and rotated BRIEF (ORB), maximally stable extremal regions (MSER) and binary robust invariant scalable key points (BRISK). In these techniques, a similarity value regarding the specified number of most important key points is utilised to determine if there is a similarity between the reference object and the objects in images, videos, or real-



Fig. 2. Interfaces of the application from top to bottom: (i) the main, (ii) training for ROI selection, (iii) training for blank set and parameter selection and (iv) recognition/splitting.

time scenes given a threshold value. No pre-processing and training is required. We tested these approaches on our sample datasets and the preliminary results indicated that none of these approaches is successful enough to detect and split very small birds with many different postures in large-scale images against the changing and complicated background of the sea (Ex: Figs. 6, 16). It is noteworthy to mention that variations in sea-state, marine environments, atmospheric conditions, and solar illumination angles combine to produce a wide range of sea surface image patterns that form the background to the targets of a bird mapping operation (Groom et al., 2013).

The other approach is the supervised ML approach, which requires prior datasets to both determine the common features and train the system for further similar detections based on these features. Accuracy rates of detection are mainly dependent on the quality of datasets used in training in terms of representing the real environment by avoiding overfitting. In the training process, general features are acquired and these features are then compared to the features of objects in test datasets to observe how well the features are detected and to determine if these features are suitable to be employed

in real life. Trained models (i.e., detectors) are used for the detection of similar objects after the evaluation is conducted successfully by using an evaluation dataset. Our preliminary tests on the sample datasets using the supervised ML approaches showed promising results, which is elaborated in Section 4.2. The frequent low numbers of marine birds in any given area adds to the complexity of developing methods for large-scale operational surveys (Groom et al., 2013). Most of the time, there might be a single gannet in a large-scale image (Ex: Fig. 16) within our surveys. This makes detecting them highly difficult with regards to splitting the images with gannets from those without gannets, for aerial surveys with more than half a million images, into the positive folder. In other words, it would be easier to detect at least one gannet among several gannets in a large-scale image rather than detecting a single gannet in the image.

To summarise, as explained above, our preliminary test results showed that employing a template matching approach did not work for detecting and splitting birds in large-scale aerial images, because, despite their distinctive features (Ex: Fig. 1) the birds are not very clear in very complex and changing sea textures despite the high quality of the images with a very high camera resolution (i.e., > 50 Megapixels). Moreover, DNN techniques do not result in satisfactory outcomes where the number of instances in domain sets is not many as in our case in this study even though they are recently popular and successfully employed in many different types of application fields and these techniques have far exceeded the accuracy rates of current ML methods. More importantly, our preliminary test using DNN showed that the misclassification of multispecies is high if data instances in different groups resemble each other too closely as seen in bird species. Therefore, we have employed an ensemble of ML and RL techniques for automated recognition, splitting, and counting of birds in aerial surveys to both reach our goals in accuracy rates and classify multispecies in the further development of the proposed application and a user-friendly application was developed using Matlab Simulink MatWorks R2020,⁵ as displayed in Fig. 2. The algorithms were developed to work on any size of bird objects using interpolation and extrapolation techniques, providing there is a training data set available. In particular, the methods of the sliding window (Forsyth & Ponce, 2012) and Gaussian pyramid (Witkin, 1984) are applied to detect any object that can appear in different regions of the image and in different scales. A detection window in the sliding window method slides over the image to extract the regions. The Gaussian pyramid (Witkin, 1984) method is primarily applied to the image during the detection stage of the sliding window to operate a scale search.

Three feature extraction techniques are employed in our methodology, namely Haar Cascades, Local Binary Patterns (LBP), and Histogram of Oriented Gradients (HOG). Each of these techniques acquires different features of objects using different mathematical modelling. We applied these techniques to establish the detectors in our implementation using Matlab ready-to-use commands along with the Viola– Jones matching

Sampling is commonly employed to census species within representative sample areas using varying sampling strategies and a way of statistical prediction or projection to a whole figure to avoid high costs

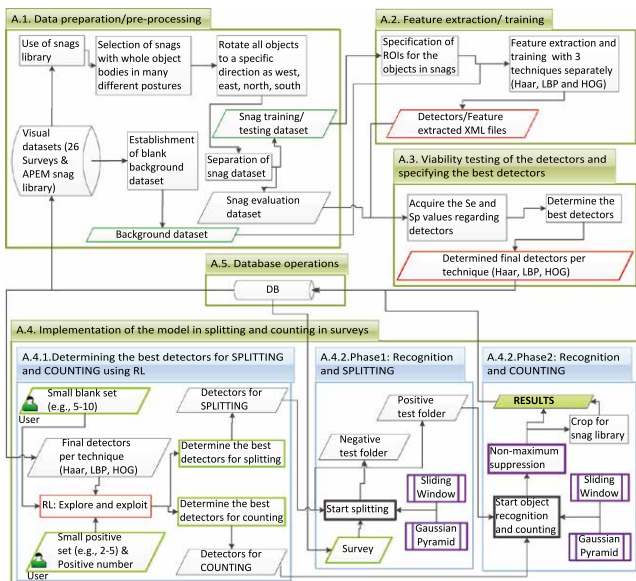


Fig. 3. Main components of the methodology.

technique.⁶ (i) Haar cascade technique resembling Haar wavelets was first introduced by Papageorgiou et al. (1998) and Viola and Jones (2001). First, the pixel values inside the black area are added together; then the values in the white area are added together. Following that, the total value of the white area is subtracted from the total value of the black area. This result is used to categorise image sub-regions (Cruz et al., 2015), which requires a fair amount of time to train a classifier and generate the Haar training set. The calculation method of Haar-like features is faster by introducing an integral image or summed-area table (Viola & Jones, 2001), which makes the computing of Haar-cascade classifiers more efficient. (ii) LBP was first introduced by Wang and He (1990) and analysed in detail by Ojala et al. (1994). It has been improved by several other studies regarding object identification and recognition (Ojala et al., 2002; Trefný & Matas, 2010; Zhang et al., 2007). In the LBP technique, the texture is

defined as a function of spatial variations in the pixel intensity of an image with a low computational cost by focusing on a small set of critical features, discarding most of the non-critical ones to increase the speed of the feature extraction and classification significantly without affecting accuracy; common features, such as edges, lines, points, flat areas, and corners can be represented by a value in a particular numerical scale (Cruz et al., 2015). Therefore, it is possible to recognise objects in an image using a set of values extracted a priori and several weak classifiers turn into a strong classifier regarding recognition (Cruz et al., 2015). (iii) HOG which explores gradient information and local shape information was first explored by McConnell (1986) and improved by Dalal and Triggs (2005). The technique counts occurrences of gradient orientation in localised portions of an image, which is computed on a dense grid of uniformly spaced cells and uses overlapping local contrast normalisation by the distribution of intensity gradients or edge directions. Due to the strong texture and shape description ability, HOG can be used in the detection of many different types of objects. It is highly sensitive to object orientation. It responds rapidly to changing parameters of FAR and TPR based on its feature extraction method which uses histograms. (iv) The Viola– Jones technique that is included in Matlab Computer Vision System Toolbox (i.e., vision.CascadeObjectDetector) is used to match acquired features in detectors to those of the objects in images for comparison and detection. This technique along with feature extraction techniques is highly sensitive to different orientations of objects in images/videos. The main reasons for choosing Viola–Jones are its fast detection speed and its high accuracy detection rate regarding the large-scale aerial images on which we are working. How these techniques are employed in a novel approach in our methodology is explored in the following sections, particularly, Sections 4.2 and 5.

The main components of the platform, WILDetect, built in this study are depicted in Fig. 3. The phases are (i) data preparation/ pre- processing (A.1), (ii) feature extraction/training (A.2), (iii) viability testing of the detectors and specifying the best detectors (A.3), (iv) implementation of the model in splitting and counting in surveys (A.4) (i.e., determining the best detectors in splitting and counting using the recursive RL approach (A.4.1), recognition and splitting (A.4.2.Phase1), recognition and counting (A.4.2.Phase2)), and (v) database operations (A.5) that are explained in the following sections respectively.

4.2. Establishment of the methodology

The defined problem space (Section 3), considering the literature analysis (Section 2) and the obtained results from the preliminary tests (Section 4.1) using off-the-shelf approaches, necessitates the development of a new approach to achieve the objectives of the research community while performing airborne wildlife census automatically in the marine ecosystem. With this in mind, the approach built here is explained step by step in the following subsections (Sections 4.2.1, 4.2.2 and 4.2.3) and the results of the implementation using large surveys are provided in Section 5).

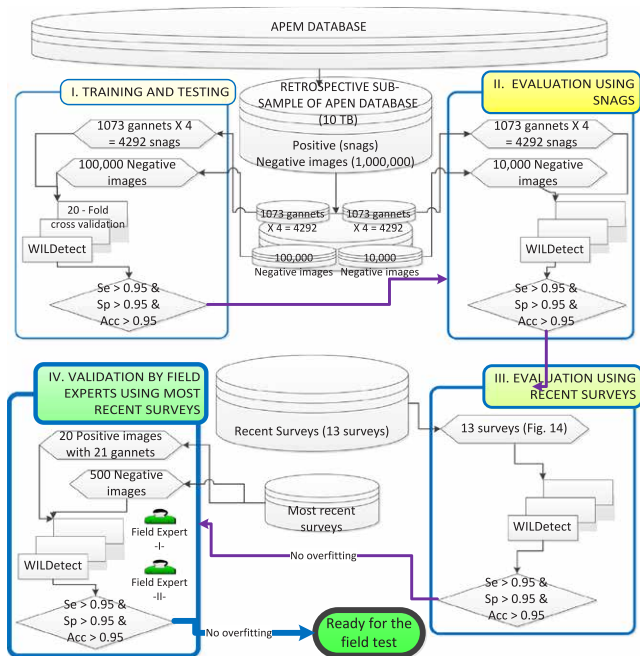


Fig. 4. Use of datasets during training, testing, evaluation, and validation of WILDetect.



Fig. 5. APEM aeroplane during a remotely-sensed aerial survey using advanced aerial high resolution photogrammetry.

4.2.1. Data sets, data preprocessing/preparation (A.1)

The main subcomponents of this phase along with their interaction are illustrated in the dedicated section of Fig. 3 titled “A.1”. A dataset consisting of images with the object of interest and a dataset consisting of blank/background images that represent anything except the object of interest are needed to establish a supervised ML approach for training, testing, evaluation, and validation. Data preparation and data management in those steps are demonstrated in Fig. 4. The negative set typically contains more images than the positive set in order to complete the training phase where every positive image needs more background images that represent the real-world environment. APEM has many surveys in its repository in which almost %95 of the images are blank background images with no targeted object types. APEM conducts offshore digital wildlife surveys for the offshore renewables sector, reliably capturing imagery all year round in all lighting conditions and sea states up to four. The data is captured on a variety of sensor formats including both 35 mm and medium format from various manufacturers, in both single camera

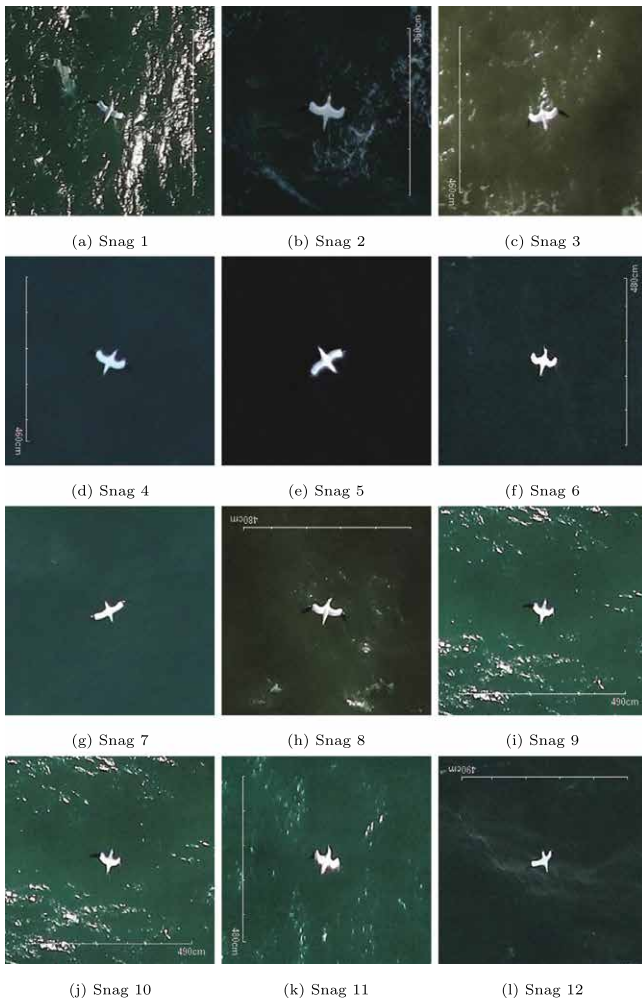


Fig. 6. Examples of the gannet snags for the north direction in several postures and background textures.

and multiple camera configurations, depending on the project requirements. The images are collected by these advanced cameras mounted in a small twin-engine aeroplane (Ex: Fig. 5) within a route in which all regions of interest are surveyed.

A snag library that consists of around 1 million snags (i.e., cropped images with objects of interest; ex: Fig. 6) has been established by APEM. We aimed to incorporate all possible targeted positive images into the methodology, either for training/testing or evaluation and validation to create a positive dataset that can represent the real-world object types by avoiding overfitting during the decision-making phase of the implementation in real-field tests. We pre-processed the gannets in this library by selecting the convenient gannet samples. Our preliminary tests showed that flying gannets with their partial body parts can be detected using whole body sets, but, a whole

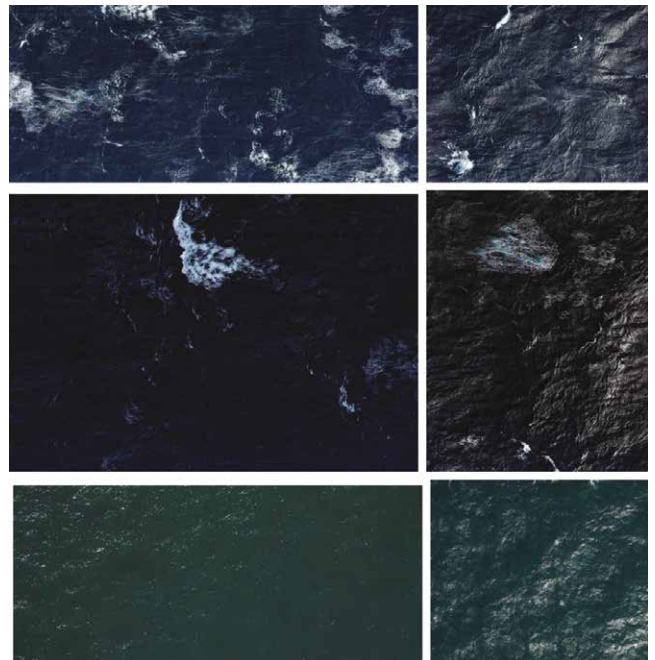


Fig. 7. Examples of blank images from 6 different surveys with various textures.

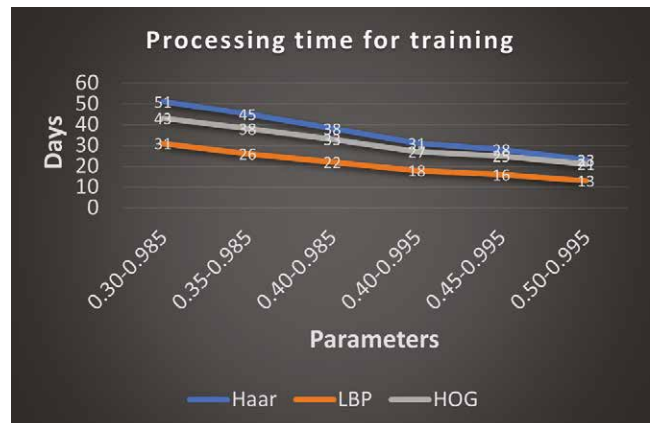


Fig. 8. Processing time of detectors in Table 1.

Table 1 Processing time of the detectors in days.

Techniques	0.30-0.985	0.35-0.985	0.40-0.985	0.40-0.995	0.45-0.995	0.50-0.995
Haar	51	45	38	31	28	23
LBP	31	26	22	18	16	13
HOG	43	38	33	27	25	21

Table 2 Accuracy rates of the training phase with the snag dataset based on the detectors with 6 different parameters: all snags are recognised successfully by the parameters, FAR = 0.50 and TPR = 0.995 with the combination of 3 techniques.

Techniques	0.30-0.985	0.35-0.985	0.40-0.985	0.40-0.995	0.45-0.995	0.50-0.995
Haar	0.825	0.975	0.98	0.985	0.989	0.993
LBP	0.675	0.925	0.935	0.966	0.984	0.992
HOG	0.735	0.85	0.9	0.993	0.994	0.994
Combined	0.84	0.99	0.992	0.995	0.996	1

gannet body cannot be detected by a trained set that consists of various partial parts of gannets (e.g., only one wing). Furthermore, partial body parts can increase the false-positive (FP) rate. Therefore, in this phase, we aim to select as many gannets as possible that have whole bodies (i.e., two wings, head, and tail), but in all possible postures. With this in mind, we prepared two sets of gannets (50%/50%), one of which is for training/testing with 1073 snags (Fig. 4I) and the other one is for evaluation with again 1073 snags in many different postures (Fig. 4II). Our preliminary test results suggest that the detectors built using the three feature extraction techniques (i.e., Haar, LBP, HOG) based on the specific orientations (i.e., north, east, south, west) improve the accuracy rate significantly where these techniques are highly sensitive to different orientations of objects in images as explained in Section 4.1. Therefore, all the gannet objects in these sets are rotated into 4 directions automatically using the codes produced in this study for the data preprocessing phase, namely, north, east, south, and west, by which 4 sets of gannet objects totalling $1073 \times 4 = 4292$ were generated for training/testing and evaluation, rather than separating them into these directions into 4 groups, which would reduce the number of objects substantially. In this way, 4 types of detectors are needed with the orientations north, south, east, and west, as well as a large number of negative images. The greater the variety of these snags/images representing the real environment, the better the detectors avoiding overfitting and consequently the higher the accuracy of detecting targeted objects in images in real field tests. A sub-sample of the dataset in which all gannets are almost rotated to the north is presented in Fig. 6. More snag examples can be found in our technical report — MarineObjects_Gannet_Supplement_2.pdf in the supplementary materials. Moreover, the gannet objects in large-scale images (Ex: Fig. 16) are presented in our technical report — MarineObjects_Gannet_Supplement_3.pdf in the supplementary materials with many different postures and background textures.

In addition to the positive dataset, a blank/background/negative dataset was established using 26 surveys collected by APEM between 2014 and 2017. These surveys were acquired from different parts of the world in different seasons and time zones using different settings and types of image-capturing technologies. The texture of the negative images in these surveys

differs from each other as displayed in Fig. 7, which makes the implementation more challenging. More examples specific to the surveys can be found in our technical report — MarineObjects_Gannet_Supplement_1.pdf in the supplementary materials. We were given around 1 million images that are the subsets of these surveys. We used this large number of surveys, a volume of around 10 TB, to find out the general characteristics of aerial surveys. The diverse features revealed from these large surveys help make our approach strong and promising for further use of the application in any circumstances while separating targeted objects from their background. This large dataset was stored in

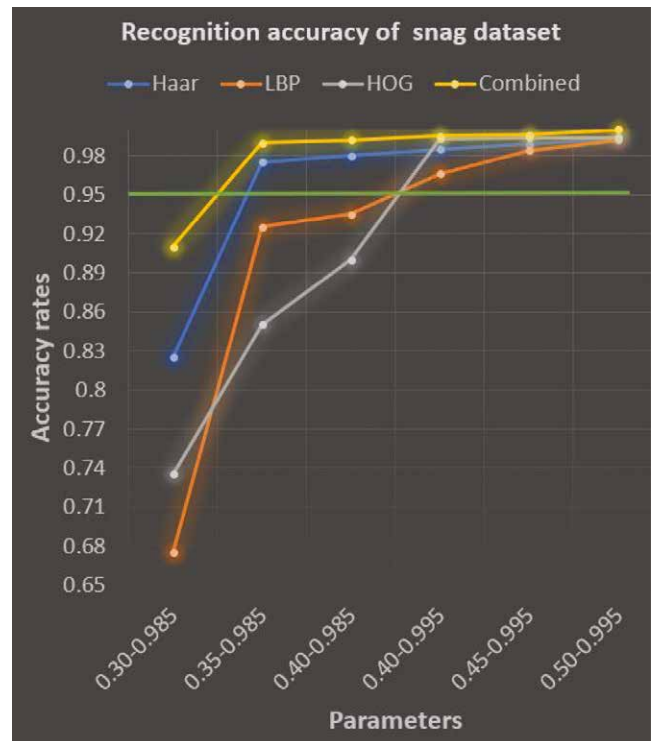


Fig. 9. Results for Table 2: The accuracy rate of recognition is increased by combining 3 techniques, which is depicted by the yellow line. Combination of 3 techniques is more important where the FAR and TPR parameters are smaller to acquire a satisfactory recognition rate. The horizontal green line drawn on 0.95 Se is the objective threshold level; the Se values over this line are acceptable in terms of the yellow line.

high-powered servers and processed using these servers (A storage unit (12 TB), 2 Novatech servers and 5 HP servers connected to each other via the network. The storage unit is used for placing the big size of the datasets and applications on servers are run using the datasets placed in the storage unit for development, evaluation and validation. The specifications of the Novatech servers: Intel (R) Xeon (R) CPU E5 26300 2.30 GHz 2.30 GHz (2 processors), 64 bit, 64 GB RAM, GPU (NVIDIA GeForce GTX 680). The specifications of the HP servers: Intel (R) Xeon (R) CPU 5160 3.00 GHz, 64 bit, 8 GB RAM. We established a sub-sample set from the diverse surveys that consisted of 100,000 images (Fig. 4I) to use in the training process, with the aim of incorporating all the characteristics of the current and future surveys into implementation. It is worth emphasising that an equal number of negative images from all sub-surveys (107 sub-surveys), within the above-mentioned 26 surveys, were included considering the seasons and time zones to create a negative dataset that can represent the real-world circumstances. Rather than using 1 million images, this sub-sampled set would reduce the processing time of training significantly, in particular, while singling out the consecutive new sets for each following training iteration, which is elaborated in Section 4.2.2. Readers are referred to Fig. 4 in the related sections below in which the evaluation and validation are explained

after revealing the establishment of the methodology in the following sections.

4.2.2. Feature extraction and training (A.2)

The main subcomponents of this phase along with their interaction are illustrated in the dedicated section of Fig. 3 titled “A.2”. Automatic detection systems usually require large and representative training datasets to achieve good detection rates with fewer FP rates (Vállez et al., 2015). The training phase is very important for the successful recognition of objects in the further use of the application. One badly trained file/classifier can cause the splitting process (A.4.2. Phase1 in Fig. 3) to function poorly and many positive images may be placed in the negative folder and vice versa, which we aim to avoid. The user interface developed for the training phase is displayed in Fig. 2ii and iii. With this interface, the detectors can be generated using several parameters such as true positive rate (TPR), false alarm rate (FAR), number of training stages, number of background images, and negative sample factor (NSF), with respect to the number of positive images in each training stage and the feature extraction techniques, i.e., Haar, LBP, and HOG. A mathematical model of the objects is extracted using these techniques as explained in Section 4.1. These techniques were selected, because, in addition to providing detectors with encouraging accuracy, they produce detectors that can function efficiently. For instance, objects can be detected in a

few seconds in an image with 50 million pixels. The training interface lets the user feed the system with positive images for ROI selection and negative images for background analysis, as well as specify the parameter values. ROIs are specified in positive images by the user (at least one ROI in each image), and the feature descriptors are extracted based on ROIs using the aforementioned techniques in the training process. Several training sets were acquired using different FAR and TPR parameters for each feature extraction technique. In each training, the number of training stages was 20 (i.e., 20-fold cross-validation) along with the number of the negative samples 3, which means that the number of the different negative images to be used in each training stage of the 20 iterations would be as many as 3 times the number of positive images. Our preliminary tests show that (1) decreasing the number of iterations (e.g., 10-fold) increases the training time significantly, (2) the recognition accuracy rate is almost the same with negative sample factors of 3 and 10; however, the processing time increases significantly with the value of 10. Therefore, the training parameters 20 for iterations rather than most commonly used 10-fold and 3 for negative sample factor were selected to decrease the training time. In each iteration, the techniques choose a set of different negative images in the negative dataset whose texture features are supposed to be different from the previously selected sets. The system stops if not sufficient negative images with different features are provided.



(a) The snag detected by only Haar technique using the trained file Haar right.

(b) The snag detected by only LBP technique using the trained file LBP down.

(c) The snag detected by only HOG technique using the trained file HOG up.

Fig. 10. Snag examples detected by only one of the techniques with the parameters of FAR = 0.35 and TPR = 0.85.

Therefore, the images in the negative dataset must be different from each other with respect to their textures. A large number of images in the negative dataset increase the chance of finding a new set for each following training iteration. As explained earlier, 100,000 images selected for the negative datasets from different surveys provide enough distinctive iteration sets for our training iteration steps.

The training process is repeated to obtain several detectors using different parameters, in particular, reducing the values of TPR and FAR to flag fewer FPs. This is mainly beneficial to the analysis of different types of surveys with regard to their varying textures, as explained in the following sections. As soon as the detectors are generated, they are tested on the sample test dataset and the threshold parameters are reduced until almost all negative images are transmitted into the negative directory. This may cause several positive images to be missed with respect to each technique with reduced threshold parameters. However, these techniques use different features and if one detector with a technique misses one positive image, there is a high probability that one of the other two detectors using the other two techniques may specify this image as a positive image. Therefore, we are employing these three techniques at the same time for the splitting phase to overcome the reduced sensitivity (Se) because of the FNs with respect to each technique in order not to miss any positive image, which is explained in Section 4.2.3 in detail with examples.

Detectors for the specific types of objects are created only once and can be used whenever needed to recognise, split and count specific objects in images for further analysis. Six trained sets — detectors consisting of 72 trained files (i.e., 6 threshold values \times 3 techniques \times 4 directions = 72) were created using 6 threshold values, as displayed in Table 1. In other words, 12 trained files were obtained for each trained set, 4 for each technique

(i.e., Haar, LBP, HOG) and each of which represents the gannet sets in one of the four directions (i.e., north, east, south, west) (i.e., 12 trained files for each detector \times 6 detectors = 72). The processing time of the training in terms of threshold values is shown in Table 1 and Fig. 8. The smaller the threshold values, the longer the training time.

4.2.3. Viability testing of the detectors and specifying min/max threshold parameters (A.3)

The acquired trained files were evaluated on the evaluation dataset (i.e., 1073 snags in four directions) spared for evaluation (Fig. 4II) as mentioned in Section 4.2.1. The evaluation results are presented in Table 2 and Fig. 9. As it is noticed in Fig. 9, the detection success of the feature extraction techniques varies depending upon the approaches followed in these techniques as elaborated in Section 4.1 as the parameters concerning the features of the datasets changed. For instance, the effect of the HOG technique is relatively poor when the parameters are small, and it increases rapidly after the values of parameters are increased. In this way, the drawbacks of one technique considering the features of data can be compensated by the other two techniques while the parameters need to be changed for achieving the desired goals, either for increasing Se or for increasing Sp . The trained files with the parameters FAR = 0.30 and TPR = 0.985 resulting in a Se value of 0.840 are excluded from the trained folder in order not to be used for further recognition and splitting process. Because the main objective of this research is to obtain a Se value greater than 0.95 which is one of the targeted success criteria, i.e., threshold level, as shown in Fig. 9 with the green line. In other words, we do not want to miss positive images at any cost even with small Sp values by achieving this success criterion. As explained in Sections 5.1 and 5.2, the system with established detectors was run on various evaluation and validation surveys (Fig. 4III and IV) with varying characteristics to find out the detectors' viability on further surveys

based on the observed Se and Sp values, strictly speaking, Sp after achieving a satisfactory Se value with 5 threshold intervals, all of which are above the targeted sensitivity value, 0.95.

The use of three feature extraction techniques at a time is more important where the detectors with smaller threshold parameters are selected by the system with the RL approach as explained in the following Section 5. Some of the gannet objects detected by only one of the feature extraction techniques are presented in Fig. 10 where FAR = 0.35 and TPR = 0.85. These three gannet objects are detected by the three techniques at the same time with bigger threshold values where FAR = 0.50 and TPR = 0.95. We would like to note that these high threshold values may cause many FPs depending on the complexity of the background and it may not be a good option to use them for particular types of surveys, which is explained in the following sections in detail.

Endnotes

¹ <https://apem-inc.com>.

² <https://www.apemltd.co.uk>.

³ Courtesy of the photographer and artist Rahul Alvares.

⁴ APEM Ltd is a leading independent environmental consultancy specialising in freshwater and marine ecology. The company is the world's leading provider of digital aerial wildlife surveys for the offshore wind industry, having carried out over 2000 surveys in the North Sea, Irish Sea, Baltic Sea, Pacific, Atlantic, and Gulf of Mexico.

© 2023 The Author(s). Published by Elsevier Ltd. This is an open access article under the CC BY license (<http://creativecommons.org/licenses/by/4.0/>).

The paper is republished with authors' consent.

To be continued in next issue. 

How ISRO used satellite remote-sensing to analyse glacial lakes in Himalayas

The Indian Space Research Organisation (ISRO) recently released satellite-data-based analysis on expansion of glacial lakes in the catchments of Indian Himalayan river basins. This is the latest among a clutch of studies on glacial lakes that have highlighted the risks of glacial lake outburst floods (GLOFs), and their impact on infrastructure and settlements downstream of such lakes.

What did ISRO's analysis reveal?

ISRO's analysis looked at satellite data archives spanning the past four decades to assess changes in the glaciated environment. Long-term satellite imagery covering the catchments of Indian Himalayan river basins — spread over India, Nepal, Tibet, and Bhutan — is available from 1984 onwards, till 2023. ISRO's data has indicated significant expansion in the size of glacial lakes.

Of the 2,431 lakes larger than 10 hectares (identified during 2016-17), 676 glacial lakes had expanded significantly since 1984. Of these 676 lakes, 601 lakes had more than doubled in size, 10 lakes had grown between 1.5 to 2 times, and 65 lakes had grown 1.5 times.

ISRO said that 130 of the 676 lakes are situated in India, in the Indus (65), Ganga (7), and Brahmaputra (58) river basins. These lakes have expanded as glaciers are retreating at an ever faster rate due to global warming.

How are glacial lakes formed?

The movement of glaciers causes erosion and creates depressions in the surrounding topography. When they retreat, meltwater starts to accumulate in such depressions, giving birth to glacier lakes.

ISRO categorised glacial lakes into four broad categories based on how they were formed — moraine-dammed, ice-dammed, erosion-based, and 'others'. Moraine and

ice-dammed lakes are formed when water is dammed by moraine — debris such as rocks and soil left during the movement of glaciers — and ice respectively. Erosion-based lakes are formed when water is dammed by erosion-created depressions.

While glacial lakes are crucial sources of freshwater for rivers, they also pose significant risks, specifically of GLOFs, which can have devastating consequences on communities downstream.

“GLOFs occur when glacial lakes release large volumes of meltwater due to the failure of natural dams... resulting in sudden and severe flooding downstream. These dam failures can be triggered by various factors, including avalanches of ice or rock,” ISRO said.

How is satellite remote-sensing technology used to monitor glacial lakes?

The monitoring of glacial lakes and their expansion in the Himalayan region is challenging due to the rugged terrain. This is where, according to ISRO, satellite remote-sensing technology “proves to be an excellent tool for... monitoring due its wide coverage and revisit capability”.

“Satellite-derived long-term change analysis provide valuable insights for understanding glacial lake dynamics, which are essential for assessing environmental impacts and developing strategies for GLOM risk management and climate change adaptation in glacial environments,” ISRO said.

Glaciologist Ashim Sattar, Assistant Professor, Indian Institute of Technology, Bhubaneswar, said: “Most of the glacial lake sites are not accessible by motorable roads. In this scenario, remote sensing tools, which are highly advanced now, can help us monitor the growth of glacial lakes and understand their dynamics”.

He also said fieldwork can be carried out at lake sites which have been identified as potentially critical. “Fieldwork is crucial to set up instrumentation for early

warning systems. These can include installing motion detection cameras, water level sensors, discharge meters etc. that can capture anomalous activity in and around glacial lakes,” Sattar said.

How can the risks posed by glacial lakes be mitigated?

In 2023, a study published in the Journal of Geophysical Research examined the risks posed by Ghepan Gath lake — located at an elevation of 4,068 m in Himachal Pradesh — to Sissu in Lahaul valley, and modelled the impacts of lowering the water levels in the lake.

It found that lowering of the lake levels by 10 to 30 m significantly reduces the impacts on Sissu town, though not completely eliminating the risks posed by a GLOM event.

One way to syphon off lake water is by using long High Density Polyethylene (HDPE) pipes. In 2016, members of the Sikkim State Disaster Management Authority and Sikkim's Department of Science and Technology and Climate Change, among others, used this method to reduce water levels in Sikkim's South Lhonak Lake. <https://indianexpress.com>

IN-SPACe releases guidelines for implementing indian space policy

Space regulator IN-SPACe recently unveiled norms, guidelines and procedures for effective implementation of the Indian space policy that opened up the sector to private players to engage in a range of activities from building and launching satellites to setting up ground stations and share remote sensing data.

The 147-page document lists out space activities that need authorisation from IN-SPACe, specifies criteria for granting such authorisations and provides necessary guidelines/pre-requisites to be fulfilled by an applicant for making an authorisation application.

The norms, guidelines and procedures (NGP) will complement the government's

endeavour in providing a predictable regulatory regime, transparency and ease of doing business in the Indian space sector. www.ptinews.com

NASA, Japan advance space cooperation

NASA Administrator Bill Nelson and Japan's Minister of Education, Culture, Sports, Science and Technology (MEXT) Masahito Moriyama have signed an agreement to advance sustainable human exploration of the Moon. Japan will design, develop, and operate a pressurized rover for crewed and uncrewed exploration on the Moon. NASA will provide the launch and delivery of the rover to the Moon as well as two opportunities for Japanese astronauts to travel to the lunar surface.

President Biden and Prime Minister Kishida also announced, "a shared goal for a Japanese national to be the first non-American astronaut to land on the Moon on a future Artemis mission, assuming important benchmarks are achieved." The pressurized lunar rover is intended to enable astronauts to travel farther and work for longer periods on the lunar surface. The signing took place April 9 at NASA Headquarters in Washington. Along with Nelson and Moriyama, JAXA (Japan Aerospace Exploration Agency) President Hiroshi Yamakawa also participated in the signing. www.nasa.gov

Muon Space and Earth Fire alliance unveil FireSat constellation

Muon Space, an end-to-end Space Systems Provider that designs, builds, and operates mission-tailored low-earth orbit (LEO) satellite constellations, in partnership with Earth Fire Alliance (EFA), has announced the FireSat Constellation. This initiative aims to transform global wildfire response and enhance climate resilience worldwide. FireSat has been developed over the last five years with the expertise and support of Google Research and leading non-governmental organizations (NGOs) including the Environmental Defense Fund (EDF), Google.org, the Gordon and Betty Moore Foundation,

and the Minderoo Foundation along with guidance from over 200 members of the federal, state, and local fire community. The FireSat Constellation will provide the most comprehensive, high-fidelity data to protect Earth's ecosystems from the escalating threat of wildfires. www.muonspace.com

ESA and Luxembourg extend space resources collaboration

ESA and the Government of the Grand Duchy of Luxembourg signed an extension of their memorandum of cooperation concerning the field of space resources for another five years, underscoring both parties' commitment to advancing sustainable and peaceful exploration beyond Earth.

Key areas of convergence include developing the space resources sector to facilitate sustainable space exploration, while fostering the creation of new markets and business opportunities as well as using the technological innovations from this field to improve life on Earth.

The extension has been signed in the context of a visit of ESA's Space Research and Technology Centre (ESTEC) in Noordwijk by the Minister of the Economy, SME, Energy and Tourism, Lex Delles. ESTEC is the European Space Agency's technical center. It is ESA's largest center where around 2,500 technicians, engineers and researchers, including Luxembourgish experts, work on space technology development and spacecraft design. meco.gouvernement.lu

First two worldview legion spacecraft performing well after launch

Maxar Intelligence has confirmed the first two WorldView Legion satellites are performing well after its recent launch on a SpaceX Falcon 9 rocket. These two satellites are part of a first block of six WorldView Legion satellites. When these six satellites join Maxar Intelligence's constellation, the business will be able to collect imagery of the most rapidly changing areas on Earth as frequently as every 20 to 30 minutes. www.maxar.com

LTIMindtree and IBM collaborate on Generative AI Centre in India

LTIMindtree announced a collaboration with IBM to establish a global, joint Generative AI Center of Excellence (CoE) in India.

The CoE plans to offer a comprehensive suite of services, combining LTIMindtree's expertise in data and machine learning model customization and full-stack engineering with IBM watsonx technology and AI assistants. newsroom.ibm.com

New mapping technology shows carbon stored in hedgerows

The Great Britain and Ireland's hedgerows have been in the spotlight over recent months, with growing awareness of their vital role in improving biodiversity and increasing carbon sequestration.

As well as providing shelter for wildlife, hedgerows capture carbon and help to reduce flooding.

Bluesky International has now developed a further layer of geospatial data which enable users to calculate the carbon storage capacity of hedgerows. It has extended its tree expertise to the National Hedgerow Map™ (NHMT™), which has the unique ability to calculate hedgerow carbon storage capacity. The dataset offers location, height, volume, vegetation extent, and the centreline for all vegetation below three metres. <https://bluesky-world.com>

Assam launches digital platform for disaster reporting

Assam state in India took a significant step towards more efficient disaster management recently with the launch of the Disaster Reporting and Information Management System (DRIMS). The digital platform has been developed in collaboration with UNICEF.

The initiative, spearheaded by the Assam State Disaster Management Authority (ASDMA), aims to streamline the process of reporting and assessing disaster impacts.

DRIMS captures critical data on damages, including crop losses and livestock deaths, allowing for the swift delivery of relief and rehabilitation grants to affected communities. www.timesofindia.com

Making gis data accessible for emergency response

Analysing geospatial data is unfortunately quite a complex task for non-specialists, especially during emergencies such as a flood. To support accessibility for everyone, Ageospatial uses natural language and human interaction to make geospatial analyses.

Their story started in January 2024, when a group of friends in Switzerland developed a plugin named 'Geo+ for ChatGPT' (formerly GeoGPT) on the ChatGPT Store. The plugin was successful, attracting 1000 users in less than a month and generating traction. It was able to do basic geospatial data operations such as generating, processing and exporting geospatial data (geocoding, clipping, country boundaries, population, buildings, satellite imagery...).

In response to the success of the plugin, Ageospatial developed 'GeoForge', a web platform to make location data (geospatial) analysis accessible for vulnerable communities, to support them in their response to their natural disaster and extreme weather event-related emergencies. This platform supports data-friendly users within authorities, responders and NGOs, insurance, and engineering firms to rapidly assess damage from natural disasters, analyze previous risks and predict the upcoming ones.

GeoForge was used for analysing a flood event in Bangladesh. In less than 30 seconds and by using a text prompt, the platform was able to display near real-time satellite imagery, and extract the flood extent. This was cross-referenced with geodata about critical infrastructure like power lines, water pipes, hospitals, roads, and rail systems as well as building and population datasets. www.itc.nl

Virtual Surveyor upgrades UAV surveying software

Virtual Surveyor has enhanced its smart UAV surveying software with new planimetric survey capabilities. Its version 9.5 allows users to quickly and accurately survey 2D features from UAV orthophotos and add them to the 3D topographic model generated from the same data set. It provides users with an end-to-end workflow to conduct 3D surveys from UAV imagery. The integrated Terrain Creator app photogrammetrically processes UAV photos to build survey-grade digital surface models (DSMs) and orthomosaics. www.virtual-surveyor.com

RapidFlight announces cutting-edge mobile production system

RapidFlight has released its customer-proven Mobile Production System (MPS). MPS enables the manufacturing and deployment of unmanned aerial vehicles (UAVs) from forward locations. It can be owned and operated by RapidFlight, or it can be used by the US Department of Defense (DoD), its allies, and defense contractor primes as an effective way to mass manufacture their UAVs anywhere in the world.

A single MPS can produce 28 Group 3 aircraft per month (or much higher quantities for Group 2 and/or Group 1). Each MPS unit can be operated independently or in coordination with other MPS units by two trained technicians. www.rapidflight.aero

Edge Autonomy upgrades UAS

Edge Autonomy has released significant upgrades to its VXE30 Stalker unmanned aerial system (UAS) through the new "Havoc" configuration, designed to double the system's flight endurance and payload capacity.

The VXE30 Stalker UAS has silent, vertical take-off and landing (VTOL) capabilities and is payload agnostic with

the Havoc configuration. It supports easy integration of third-party payloads and subsystems through a Modular Open Systems Approach (MOSA), requiring no additional training for current operators. edgeautonomy.io

NOAA, Verizon Frontline enhance storm damage assessment

NOAA and Verizon Frontline signed a three-year Cooperative Research and Development Agreement (CRADA) to explore new strategies to rapidly deploy uncrewed aircraft systems that will collect and distribute imagery of damage resulting from severe storms such as tornadoes and hurricanes.

As part of this partnership, the Verizon Frontline Crisis Response Team will provide the uncrewed aircraft system platform, sensor, and personnel resources needed to rapidly respond and collect aerial imagery of storm-damaged areas of interest identified by NOAA.

The goal is to enhance the ability of NOAA's National Weather Service offices to quickly conduct post-storm damage assessments, while also providing data for research conducted by the NOAA National Severe Storms Laboratory. research.noaa.gov

Pix4D upgrades PIX4Dcatch

Pix4D have launched PIX4Dcatch 2.0. This new and improved version of Pix4D's terrestrial scanning iOS mobile app adds professional-grade augmented reality (AR) and compatibility with a multitude of RTK devices. It is an easy-to-use mobile 3D scanning and AR visualization tool.

With the 2.0 update, PIX4Dcatch gains professional-grade AR features that enable interaction with a site in real time. Using AR, plans can be overlaid on-site and visualized for rapid approval during project design, construction, and post-construction inspections. 

Calian introduces TW5387 Smart GNSS antenna

Calian released a new model of Industrial Grade Smart GNSS Antennas, the TW5387. TW5387 incorporates the ST TESEO V GNSS receiver chipset (Quectel Module) onto the Calian compact (60 mm) Smart GNSS Antenna platform offering dual band GNSS, eXtended Filtering, low Phase Centre Variation, Low Signal to Noise Ratio, Dual Feed Dual Patch for strong multi-path rejection. The TW5387 is capable of enhancing its excellent standalone performance with RTK Rover capability and a built-in Inertial Measurement Unit (IMU) for Sensor Fusion. www.tallysman.com

Shift5 introduces GPS integrity module

Shift5 has released the Shift5 GPS Integrity Module, the first known platform-agnostic solution applicable for military, aviation, rail, maritime, and space industries. With real-time access and analysis of onboard data, the patent pending GPS Integrity Module assesses changes in navigational position through multi-faceted anomaly detection methods, alerting operators to GPS spoofing attacks as they happen. The GPS Integrity Module enables operators today to make smarter, faster, and safer decisions at the edge based on automated detection capabilities to mitigate risks involving the manipulation of GPS signals to help ensure the accuracy and reliability of navigation. shift5.io

Spirent announces PNT X

Spirent Communications plc has announced PNT X, its next-generation positioning, navigation and timing (PNT) simulation system. It offers the highest fidelity and most signal sources in a single test platform to address the future of enhanced autonomy, safety, efficiency, and precision.

As developers look beyond GNSS alone to address increasingly complex positioning challenges, PNT X brings together signals

including L-band, S-band, and alternative navigation (AltNav) signals, as well as industry-first Regional Military Protection (RMP) support. www.spirent.com

Leica Geosystems launches its first machine smart antenna

Leica Geosystems has launched Leica iCON GPS 120 — a smart antenna designed to further empower construction professionals with scalable and flexible machine control solutions. The new Smart Antenna is integrated into the existing Leica MC1 solution platform. It extends the machine control solution offering to more applications and machine types. Construction machines like compaction rollers, which usually require only sub-metre accuracy without heading, can now be equipped with a tailor-made Leica MC1 machine control solution. hexagon.com

Rohde & Schwarz, XipLink partnership

ipoque, a Rohde & Schwarz company announced its partnership with XipLink. The technology partnership sees the creation of the XipLink Application Classification Engine (XipACE) by integrating ipoque's cutting-edge DPI technology R&S@PACE 2 into the XipLink operating system (XipOS), delivering advanced application visibility for multi-orbit networking.

Leveraging standards-based SCPS protocol acceleration, link bonding, Layer 2 switching and Layer 3 routing, XipLink delivers intelligent multi-orbit networking that ensures network performance and QoS across satellite, cellular and wireless networks. www.xiplink.com

NextNav petitions FCC for new spectrum band

NextNav has filed a rulemaking petition asking the Federal Communications Commission to deliver an innovative spectrum solution in the Lower 900 MHz band (902-928 MHz band). The petition proposes rearranging the band to facilitate a terrestrial PNT network and broadband.

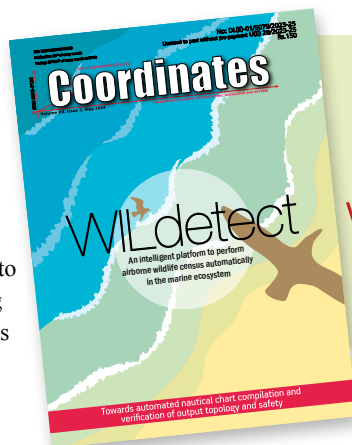
The petition specifically asks the FCC to reconfigure the band plan and adopt new rules to:

- Enable a high-quality terrestrial complement and backup to the GPS on which the nation relies for essential PNT services.
- Provide 15 megahertz of low-band spectrum for use by mobile broadband networks.

NextNav recently announced that it had signed an agreement to acquire spectrum licenses covering an additional 4 MHz in the lower 900 MHz band from Telesaurus Holdings GB LLC and Skybridge Spectrum Foundation. nextnav.com

VIavi launches resilient PNT solution

Viavi Solutions Inc. announced the availability of SecurePNT™ 6200 with SecureTimeSM services, a resilient timing clock solution that delivers the most comprehensive assurance of positioning, navigation and timing (PNT) services used in critical infrastructure operations worldwide. SecurePNT and SecureTime build on VIavi's proven assured PNT solutions with the addition of the Fugro AtomiChron® timing service, enabling intelligent zero-trust multisource assurance combining signals from Geosynchronous



Download your copy from www.mycoordinates.org

SUBSCRIPTION FORM

YES! I want my **Coordinates**

I would like to subscribe for (tick one)

1 year 2 years 3 years

12 issues

24 issues

36 issues

Rs.1800/US\$140

Rs.3400/US\$200

Rs.4900/US\$300

*

**SUPER
saver**

First name

Last name

Designation

Organization

Address

.....

City Pincode

State Country

Phone

Fax

Email

I enclose cheque no.

drawn on

date towards subscription

charges for Coordinates magazine

in favour of 'Coordinates Media Pvt. Ltd.'

Sign Date

Mail this form with payment to:

Coordinates

A 002, Mansara Apartments

C 9, Vasundhara Enclave

Delhi 110 096, India.

If you'd like an invoice before sending your payment, you may either send us this completed subscription form or send us a request for an invoice at iwant@mycoordinates.org

* Postage and handling charges extra.

34 | **Coordinates** May 2024

MARK YOUR CALENDAR

June 2024

GEO Business 2024

05 - 06 June

London, UK

<https://www.geobusinessshow.com>

ICL-GNSS 2024

25-27 June

Antwerp, Belgium

<https://events.tuni.fi/icl-gnss2024>

Training on Glacier studies and Remote sensing

18-28, June 2024

Indian Institute of Science,
Bengaluru, India

<https://iisc.ac.in>

July 2024

IGS 2024 Workshop

01-05 July in 2024

Bern, Switzerland

<https://igs.org>

Esri User Conference

15 - 19 July 2024

San Diego, CA, USA

www.esri.com

August 2024

International Geographical Congress 2024

24 - 30 August

Dublin, Ireland

<https://igc2024dublin.org>

September 2024

ION GNSS +

16-20 September

Baltimore, USA

<https://www.ion.org/gnss/index.cfm>

2024 GEO Symposium and Open Data & Open Knowledge Workshop

23 - 26 September 2024.

Hangzhou, China

<https://earthobservations.org/events>

Intergeo 2024

24-26, September

Stuttgart, Germany

<https://www.intergeo.de>

12th International FIG Workshop on the Land Administration Domain Model & 3D Land Administration

24 - 26 September 2024

Kuching, Malaysia

<https://gdmc.nl/3DCadastres/workshop2024>

November 2024

Trimble Dimensions

11-13, November 2024

Las Vegas, USA

www.trimble.com

GeoWorld

26 - 28 November 2024

Dubai, UAE

www.geoworldevent.com

Orbit (GEO), Low Earth Orbit (LEO) and Medium Earth Orbit (MEO) GPS and GNSS constellations. www.viavisolutions.com

MerlinTPS, Bluespec accelerate complementary PNT

MerlinTPS has partnered with Bluespec to address the need for GNSS augmentation and backup technology as satellites continue to face new challenges, including wartime contested space as well as increased costs to produce and maintain satellites. Under the partnership, MerlinTPS will develop its platform to support the expansion of PNT security capabilities by using existing signals of opportunity on the ground designed to combat jamming and spoofing. merlintps.com

Topcon, Bentley Systems partnership

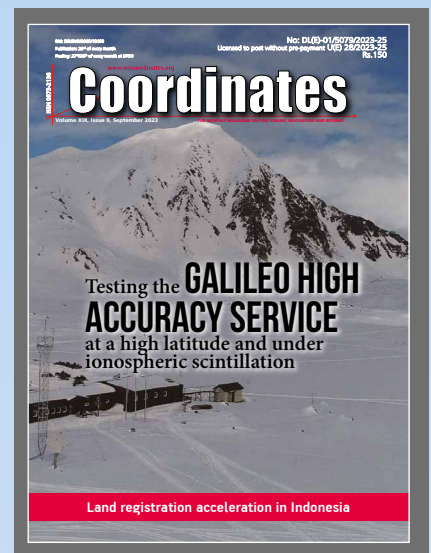
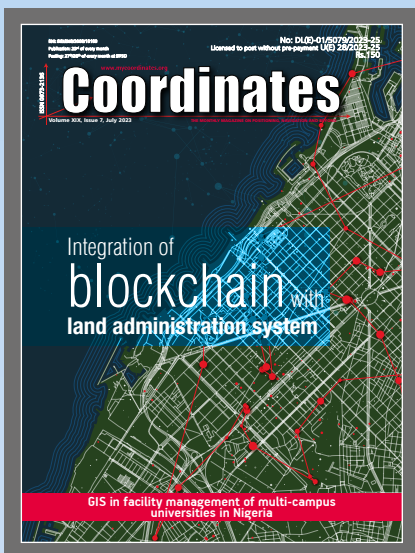
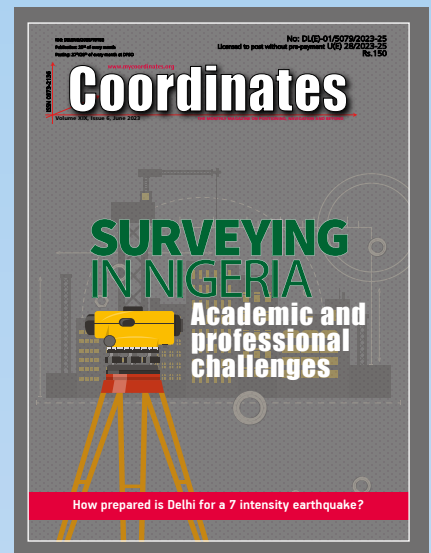
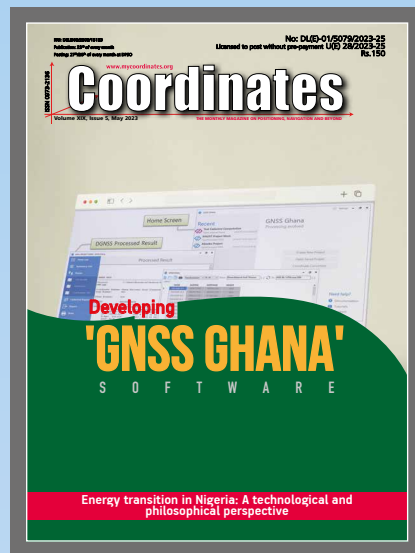
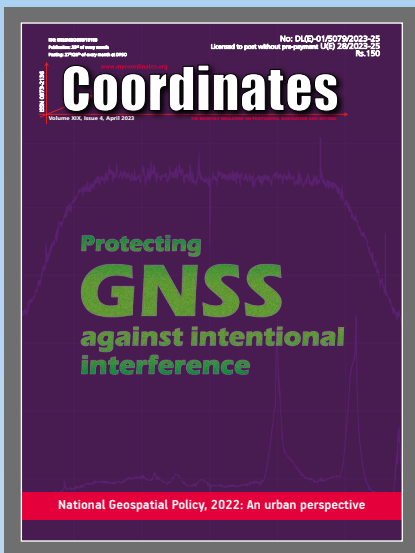
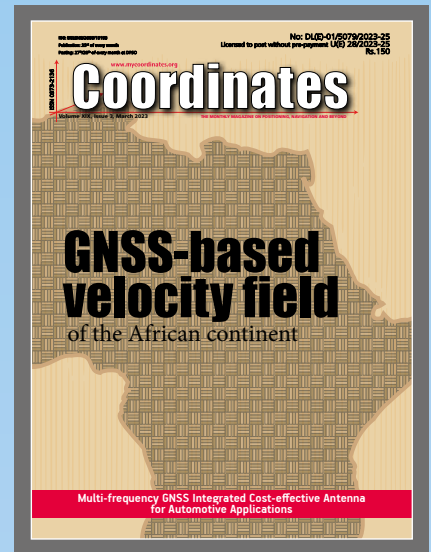
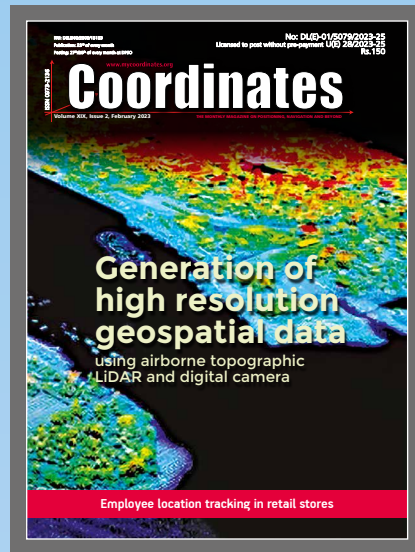
Topcon Positioning Systems has entered a strategic partnership with Bentley Systems and Worldsensing to integrate Topcon's GNSS technology into the companies' software and connectivity solutions to improve geospatial data accuracy and operational efficiency.

Under the agreement, Topcon's web-based GNSS processing engine will be incorporated into Bentley's iTwin internet-of-things (IoT) monitoring solutions, offering users real-time geospatial intelligence for better decision-making and operational effectiveness. www.topconpositioning.com

New Diamond DA62 MPP SurveyStar for the RIEGL Test Aircraft Fleet

The new DA62 MPP SurveyStar has been delivered by Diamond Aircraft Austria to RIEGL Laser Measurement Systems and it will be immediately implemented for test and calibration flights.

RIEGL and Diamond Aircraft Austria have been collaborating for almost 20 years. Since 2007, RIEGL has owned and operated the proven DA42 MPP GeoStar, which has successfully completed all missions to date with the utmost satisfaction. The increased requirements in recent years have now made it necessary to "upgrade" to the new DA62 MPP SurveyStar. ▽



“The monthly magazine on Positioning, Navigation and Beyond”
Download your copy of Coordinates at www.mycoordinates.org



0.05°
ATTITUDE

0.02°
HEADING

1 cm
POSITION

NEW ELLIPSE-D

The Smallest Dual Frequency & Dual Antenna INS/GNSS

- » RTK Centimetric Position
- » Quad Constellations
- » Post-processing Software



Ellipse-D
RTK Dual Antenna



Ellipse-N
RTK Single Antenna



OEM
RTK Best-in-class SWaP-C